CHAPTER TWO

Application Of The Box-Behnken Experimental Design To The Construction, Mechanistic Evaluation And Optimization Of The Pore-Regulated Polymer Matrices For Sustained Transbuccal Drug Delivery

2.1. INTRODUCTION

The recent resurgence in advanced developments with drug delivery systems intended for applications through various routes of administration as a result of offered advantages such as better safety profiles, bioavailability and improved patient compliance has prompted the curiosity of researchers. The importance of selecting an appropriate method of formulation of these delivery systems cannot be over-emphasized (Nadig, 2002; Li, *et al.*, 2005). The invention of a sample preparation method will influence the method's accuracy, repeatability, inter-laboratory reproducibility, simplicity, adaptability, safety, time consumption and cost-effectiveness (Nadig, 2002).

The method of formulating the pore-regulated matrix (P-RPM) can be adapted to suit its use as a rate-controlled, transbuccal drug delivery system. This is based mainly on the comprehension of the fabrication procedure which has the capability of influencing the physicochemical and physicomechanical properties of the P-RPM thereby modifying its overall behaviour. This fundamental experimental phase may pose some needless challenges if approached using the one-variable-at-a-time (OVAT) approach of scientific analysis. The OVAT approach is an un-systematic technique which involves separately changing the levels of each formulation or synthesis variable at a time and keeping all other variables constant in order to investigate the effects of specific variables on the selected response. Furthermore, this technique is inefficient and uneconomical as it is time consuming and does not provide defined information about possible interactions between factors. It can at its best lead only to a limited optimum system and in most cases, calls for unnecessarily numerous experimental runs that are not compatible with the rapidly rising costs of materials and often rely mainly on the experience of the researcher (Kincl, *et al*., 2005).

Consequently, it becomes crucial that the development of the method of fabrication and optimization of the P-RPMs be accurately performed with as few experiments as possible. This can be achieved by using the high resolution, mathematically and statistically robust, quadratic Box-Behnken experimental design. It is an efficient mathematical approach applied to determine the optimum level of each of the significant parameters (independent variables) that maximizes or minimizes the desired response and also the new factors that can be added (Goupy, 2005; Nutan *et al.*, 2005)**.** The Box-Behnken design is economical and therefore makes it particularly useful in reducing the number of experimental runs (Abdel-

Fattah *et al.*, 2005; Kincl *et al.*, 2005; Nutan *et al.*, 2005). It is one of the most efficient experimental design methods with an advantage of not containing combinations for which all factors are simultaneously at their highest and lowest levels. This makes the Box-Behnken design useful in avoiding experiments performed under extreme conditions for which inadequate outcomes are often obtained (Ferreira *et al*., 2007; Guo *et al*., 2008). Its effectiveness and reliability have been documented for the formulation of a wide range of pharmaceutical dug delivery systems (Dayal *et* al., 2005; Nutan *et al*., 2005; Chopra *et al*., 2007; Zidan *et* al., 2007; Guo *et al*., 2008; Li *et al*., 2008).

In summary, this Chapter focuses on the construction and mechanistic evaluation of the P-RPM formulations which was performed by investigating the impacts of formulation variables on their physicochemical and physicomechanical characteristics. Phenytoin sodium (PS), a class I drug according to the Biopharmaceutics Classification System (BCS) was used as the model drug for this experimental phase because of its higher aqueous solubility (100mg/mL at 25°C) and lower permeability (log P =2.14) (Darwish *et al*., 1996; Kasim *et al*., 2004) as compared to carbamazepine, the other model drug employed in the later stages of this investigation which belongs to the BCS class II demonstrating lower aqueous solubility of 0.01mg/mL at 25°C and higher permeability (log P = 2.93) (Kasim *et al*., 2004; Koester *et* al., 2004; Dong *et al*., 2007). These physical properties of PS can enable it display a higher tendency of eliciting the burst effect and possibly minimize its permeation capacity through the mucosa surface which makes it more suitable for determining the sustained drug delivery and permeation capabilities of the P-RPM formulations. Furthermore, the statistical optimization of the physicochemical and physicomechanical properties of the P-RPMs for plausible systemic drug delivery through the transbuccal route was undertaken. This whole phase was systematically conducted utilizing the Box-Behnken experimental design.

The measurement of relevant physicochemical quantities such as formulation weight and physical appearance, *in vitro* drug release behaviour, drug loading capacity, *ex vivo* bioadhesive strength, rheological assessments, surface morphology, *ex vivo* permeation efficiency, qualitative and quantitative evaluation of matrix porosity as well as some physicomechanical parameters namely the matrix resilience, energy of matrix deformation and matrix firmness/rigidity were performed. The impact of pore-regulation, measured by changes in average pore diameter and cumulative surface area of pores on the magnitude of selected physical properties (drug release, *ex vivo* drug permeation, peak force of

detachment which is a measure of bioadhesion, drug loading capacity and matrix resilience (which is a measure of physicomechanical strength) of the P-RPMs was also evaluated employing linear/non-linear mathematical expressions.

In addition, the time frame for *in vitro* drug release and *ex vivo* permeation was set at eight hours for approximately 100% drug release and permeation to enhance patient convenience and compliance during the use of this formulation.

2.2. EXPERIMENTAL SECTION

2.2.1. Materials

Chitosan (food grade) and menthol were obtained from Warren Chem Specialties, Johannesburg, South Africa. Gelatin, phenytoin sodium, polyvinyl alcohol (molecular weight = 72,000) and magnesium stearate were purchased from Sigma Chemical Company (St. Louis, USA). Span 80 (Sorbitan ester 80) and ethanol (95%) were procured from Merck Chemicals (Darmstadt, Germany) and Saarchem (Johannesburg, Gauteng, South Africa) respectively. Carbopol 974P NF was acquired from Noveon, Inc, (Cleveland, Ohio, USA). Ethylcellulose (Ethocel® 10) was obtained from Protea Industrial Chemicals (Pty) Ltd (Wadesville, South Africa). Hydroxyethylcellulose (HHX 250 Pharm) was purchased from Hercules, Aqualon (Germany). All other reagents utilized were of analytical grade and used as received.

2.2.2. Preparation of the pore-regulated polymer matrices (P-RPMs) in accordance with the Box-Behnken experimental design template

Fifteen P-RPM formulations were prepared using various combinations of independent variables by the processes of interphase, co-particulate, co-solvent, homogenization, pre-freezing and lyophilization guided through a two-level, three factor and three centre points Box-Behnken quadratic design using Minitab Statistical Software, Version 14 (Minitab Inc., State College, PA, USA). Three categories of independent variables composed of the solutes, solvents and surfactant, Span 80, were employed in fabricating the P-RPMs and were based on a statistically and mathematically generated Box-Behnken design template. The independent variable included:

(i) The water-based co-particulate dispersion (WCD) composed of polyvinyl alcohol (PVA), hydroxyethylcellulose (HEC), carbopol 974P NF (CARB), gelatin (GEL) and deionized water (DW)

(ii) The ethanol-based co-particulate dispersion (ECD) made up of ethylcellulose (ETH), magnesium stearate (MS), menthol (MTH), Chitosan (CHTS) and ethanol (EtOH) and

(iii) Span 80 (SP 80).

Each compound employed in the fabrication of the P-RPM and the rationales for their selection are outlined in Table 2.1. Combinations of both polymeric and non-polymeric additives were employed in the fabrication of the P-RPMs in order to facilitate the development of an effective formulation with optimum physicochemical and physicomechanical performance qualities suitable for the intended application as a transbuccal delivery system.

Tables 2.2 and 2.3 present the two levels of the independent variables employed and the experimental design template for the 3 factors, 3 centre points and 15 experimental runs respectively. The lower and upper limits for the factors were set based on their ability to form stable, robust drug loaded P-RPMs using minimal quantities of the individual components.

Table 2.1: The role of/rationale for selecting each compound employed in the construction of the P-RPMs

Component	Rationale for Selection and Function
Chitosan	Permeation enhancer and bioadhesive agent (Şenel and Hincal, 2001; El-Kamel, *et al.,* 2002)
Menthol	Flavor and permeation enhancer (Hamasaki, *et al*.,1998; Ho, *et al.*, 1998)
Gelatin	Matrix binder (Girhepunje, *et al*., 2009)
Polyvinyl alcohol	Stabilizer and hydrophilic matrix thickener (Olayo *et al*., 1998; El-hefian *et* al., 2010)
Magnesium stearate	Plasticizer (Swaminathan and Kildsig, 2001)
Span 80	Surfactant and permeation enhancer (Naskar *et al*., 2006; Hindustan *et al*., 2010)
Carbopol	Bioadhesive agent (Tang *et al*., 2005)
Ethylcellulose 10	Hydrophobic matrix filler, release retardant and flavor fixative (Sajeev *et al*., 2002; Emeje *et* al., 2006; Lai *et* al., 2010; Rasool *et* al., 2010)
Hydroxyethylcellulose	Homogenous blend stabilizer (Olayo *et al*., 1998)
Deionized water	Hydrophilic solute dispersant and pore originator (porogen) (Badiger *et* al., 1993; Ghosh *et al.,* 2007).
Ethanol	Hydrophobic solute dispersant and pore originator (porogen) (Schweiger *et al*., 2009)

Table 2.2: Levels of the independent variables employed in the Box-Behnken design template

Independent Variables	Levels		Units
	Low	High	
WCD [a]	0	2	mg/mL of water
ECD [b]	3	5	mg/mL of ethanol
SP 80 [c]	0.3	0.7	mL

[a] Water-based co-particulate dispersion; [b] Ethanol-based co-particulate dispersion; [c] Span 80

Table 2.3: Box-Behnken template for the preparation of each pore-regulated polymer matrix

Formulation	Composition		
	WCD (mg/20, 25 or 30 mL) [a]	ECD (mg/13, 11 or 7mL) [b]	SP 80 (mL) [c]
1	0	5	0.5
2	0	3	0.5
3*	1	4	0.5
4	0	4	0.7
5*	1	4	0.5
6	1	3	0.3
7	1	5	0.7
8	2	3	0.5
9	1	5	0.7
10	2	4	0.3
11*	1	4	0.5
12	2	5	0.5
13	2	4	0.7
14	1	5	0.3
15	0	4	0.3

[a, b, c] *Same as defined for Table 2.2;* * *Centre points for the experimental design template*

Note:

WCD: *0 - PVA (800mg) + HEC (350mg) + GEL (400mg) + CARB (100mg) + DW (30mL);*
1 - PVA (475mg) + HEC (525mg) + GEL (350mg) + CARB (150mg) + DW (25mL);
2 - PVA (300mg) + HEC (700mg) + GEL (300mg) + CARB (200mg) + DW (20mL).

ECD*: 3 - CHTS (550mg) + MS (350mg) + MTH (200mg) + ETH 10 (400mg) +EtOH (13mL);*
4 - CHTS (425mg) + MS (325mg) + MTH (250mg) + ETH 10 (500mg) +EtOH (11mL);
5 - CHTS (300mg) + MS (300mg) + MTH (300mg) + ETH 10 (600mg) +EtOH (7mL)

On the average, 25 P-RPMs were produced per batch using various quantities of WCD, ECD and SP 80 described earlier by the process of interphase co-particulate, co-solvent homogenization. The combinations of both polymeric and non-polymeric solutes, WCD and ECD, were separately dispersed in the two polar protic solvents, water and ethanol respectively. Each matrix contained 50mg PS which was dispersed in the water based medium (WCD). The two dispersions (WCD and ECD) were mixed together and the respective quantities of SP 80 (Table 2.3) were used to reduce the surface tension of the

solutes and solvents to enhance homogenization to form a stable blend with a single continuous phase. Overall, the formation of the homogenous co-particulate blend was aided with a laboratory scale homogenizer (Polytron® 2000, Kinematica AG, Switzerland) for 10 minutes (Figure 1.3 in Chapter One). The resulting blend was then cured for 30 minutes in the dark to enhance solute-solvent physical intermolecular interactions to occur. For each P-RPM, 1mL of the blend produced was pipetted into specialized, pre-oiled (employing inert liquid paraffin) polystyrene moulds (10mm diameter by 10mm height). Formulations were pre-frozen at -72 ^{o}C for 24 hours to aid the formation of the homogenous blend and then subjected to lyophilization by placing them into a freeze dryer (Bench Top 2K, Virtis, New York, USA) set at -55 ± 2°C and 0.42mBar for 48 hours. Post lyophilization, produced P-RPMs per batch were stored away for further testing in closed glass jar with active silica-containing desiccant bags.

2.2.3. Physical examination of the P-RPMs

The overall physical appearance were assessed visually and the final dry weights of the 15 formulations post lyophilization were measured utilizing a laboratory weighing balance (Mettler Toledo, AB104-S, Microsep Pty Ltd, Switzerland). This was carried out to produce data that can be employed to generate the eventual optimal weight of the P-RPM.

2.2.4. Evaluating the *in vitro* drug release behaviour of the P-RPMs

Drug release was conducted by immersing each formulation into 25mL of simulated saliva of pH 6.8 (disodium hydrogenphosphate - 2.380g, potassium dihydrogenphosphate - 0.190g, sodium chloride – 8.000g, phosphoric acid - 0.3mL added to deionized water - 1L) (Peh and Wong, 1999) contained in closed 100mL capacity glass jars. For studies at the specified conditions, three replicate samples of the individual matrices were maintained at 37±0.5^{o}C and 20rpm in a shaking incubator (Orbital Shaker Incubator, LM-530, Lasec Scientific Equipment, Johannesburg, South Africa). 3mL dissolution samples were manually withdrawn at specific time intervals over 8 hours (30, 60, 120, 240, 360, and 480 minutes) and filtered through a 0.45µm pore size Cameo Acetate membrane filter (Millipore Corporation, Bedford, MA, USA). The sink conditions were maintained by replacing withdrawn volume with freshly prepared simulated saliva at each sampling time. The amount of PS released was determined utilizing the Ultraviolet Spectrophotometer (Cecil CE 3021, 3000 Series, Cecil Instruments, Cambridge, England) at λ_{max} = 206nm.

2.2.5. Computation of the percentage drug loading capacity

The drug loading capacity (DLC) was calculated using equation 2.1. This parameter was an indication of the drug loading efficiency of the P-RPMs.

$$\% \text{ DLC} = \frac{A_d}{T_d} \text{ X } 100 \qquad \textit{(Equation 2.1)}$$

Where DLC = drug loading capacity (%w/w), A_d = actual amount of drug loaded (mg) and T_d = theoretical amount of drug loaded (mg).

For each determination, a P-RPM was completely dissolved in 100mL simulated saliva solution (pH 6.8) with the aid of the Polytron® 2000 laboratory homogenizer (Kinematica AG, Switzerland). 2mL sample was then manually withdrawn and filtered through a 0.45µm pore size Cameo Acetate membrane filter (Millipore Corporation, Bedford, MA, USA). Appropriate dilutions were carried out and samples were then analyzed utilizing the Ultraviolet Spectrophotometer (Cecil CE 3021, 3000 Series, Cecil Instruments, Cambridge, England) at 206nm. The absorbance values (y) generated were fitted into the linear polynomial equation (*$y = 16.516x$; $R^2 = 0.995$)* of the calibration curve obtained for PS. The outcome of this computation generated the actual amount of drug loaded (A_d) from the obtained concentration values (x) and was then substituted into Equation 2.1 above to generate the percentage drug loading capacity for each formulation. All evaluations were conducted in triplicate.

2.2.6. *Ex vivo* permeation studies utilizing the porcine buccal mucosa

2.2.6.1. Tissue collection and preservation

The porcine buccal mucosa was obtained from the cheek region of freshly slaughtered domestic pigs from a regional abattoir (Mintko Meat Packers, Krugersdorp, Johannesburg, South Africa). After collecting the mucosal specimens, they were immediately conveyed in a refrigerated transport box and transferred to our *in vivo* laboratory within 1 hour. The pig's buccal mucosa was specifically selected for this study because they have non-keratinized buccal mucosa similar to that of human beings. In fact, the oral mucosa of pigs resembles that of humans more closely than any other animal in terms of structure and composition (Sudhakar *et al*., 2006).

Excess connective and adipose tissues were trimmed away (using surgical scalpel and scissors) from the harvested buccal mucosal specimens. The average porcine buccal mucosal thickness employed throughout the study was 0.9±0.1mm. This was measured using a manually operated vernier caliper (25 × 0.01mm capacity). Subsequently, the trimmed specimens were snap frozen in liquid nitrogen and stored at -70°C for up to 2 months. Researchers have reported that freezing tissue specimens (either snap freezing with liquid nitrogen or the standard freezer) does not change their diffusion or permeation behaviour when used for such studies (Van der Bijl *et al*., 1998; Van Eyk and Thompson, 1998; Van Eyk and Van der Bijl, 2004; Consuelo *et al*., 2005; Giannola *et al*., 2007).

2.2.6.2. Preparation of the porcine buccal tissue specimen for permeation studies

Before conducting each permeation experiment, the frozen buccal mucosal specimens were thawed and re-hydrated to regain elasticity temporarily lost when frozen for 2 seconds in 100mL phosphate buffered saline (PBS, pH 7.4) at room temperature (21±0.5°C). The PBS solution was changed every 30 minutes with a fresh solution. After re-hydration, mucosal disks (diameter =1.5±0.1cm and surface area =2.27±0.81cm^2) were cut using surgical scissors from the harvested specimen and carefully mounted (immediately after dissection to prevent tissue rupture) on the flow through Franz type diffusion cells (Membrane transport systems, V3, Permegear, Amie Systems, USA) connected to a water bath with a circulating heating system (CPE 100, Labcon, Maraisburg, Gauteng, South Africa). The receiver compartment contained 10mL simulated plasma of pH 7.4 (disodium hydrogenphosphate - 0.795g, potassium dihydrogenphosphate - 0.144g, sodium chloride - 9g added to deionized water - 1L) (Giannola *et al*., 2007) while the donor compartment contained a 2mL solution of the drug-loaded P-RPM formulation in simulated saliva, pH 6.8 (Peh and Wong, 1999). Uniform mixing within the receiver compartment was achieved by magnetic stirring. Permeation studies were conducted in triplicate for each formulation at 37±0.5°C. At pre-determined time intervals over 8 hours (30, 60, 120, 240, 360, 480 minutes), 2mL sample volume was withdrawn from the receiver compartment of each cell and replaced with the same volume of fresh simulated plasma. Withdrawn samples were assayed for PS at 206nm on the Cecil CE 3021 spectrophotometer.

The drug flux values (J_s), through the membrane, were calculated at the steady state per unit area by linear regression analysis of permeation data following Equation 2.2 (Giannola *et al*., 2007; Minghetti *et al*., 2007).

$$J_s = \frac{Q_r}{A \times t} \qquad \textit{(Equation 2.2)}$$

Where J_s is the drug flux (mg cm^{-2} min^{-1}), Q_r is the quantity of PS that passed through the porcine buccal mucosa into the receptor compartment (mg), A is the active cross-sectional area accessible for diffusion (cm^2) and t is the time of exposure in minutes.

Also, the permeability coefficient (κ_p) (cm min^{-1}) was calculated by Equation 2.3.

$$\kappa_p = \frac{J_s}{C_d} \qquad \textit{(Equation 2.3)}$$

Where J_s is the flux calculated at steady state (Equation 2.2), C_d is the drug concentration in the donor compartment (mg cm^{-3}).

2.2.7. *Ex vivo* assessment of bioadhesive capacity using porcine buccal mucosa

The *ex vivo* bioadhesive strength of the P-RPMs were determined using a calibrated Texture Analyzer (TA.*XTplus*, Stable Micro Systems, Surrey, England) fitted with a cylindrical stainless steel probe (10mm diameter) and freshly isolated porcine buccal mucosa (diameter =1.5±0.1cm and surface area =2.27±0.81cm^2) as the model tissue. All measurements were done in triplicate. The buccal mucosa was attached to the cylindrical probe while the P-RPM was mounted onto the texture analyzer stage. The two surfaces were properly aligned to ensure that they came into direct contact with each other during measurements. The settings employed during testing were: contact force (0.1g), pre-test speed (2mm/sec), test speed (0.5mm/sec), post-test speed (10mm/sec), applied force (102g or 1N), return distance (8mm), contact time (10s), trigger type (auto) and trigger force (5g or 0.049N).

For each measurement, the surface of the porcine buccal mucosa was made evenly wet by soaking into 2mL simulated saliva placed in a glass Petri dish for 5 minutes. Subsequently, the tissue was lowered towards the formulation on the stage to make contact. Bioadhesive strength was calculated from the generated force-distance curve as the peak detachment force (F_{det}) measured in Newton (N) and work of adhesion (ω_{adh}) in Joule (J). The peak detachment force was taken as the maximum force needed for detaching the matrix from the

tissue while the work of adhesion was calculated as the area under the force-distance curve

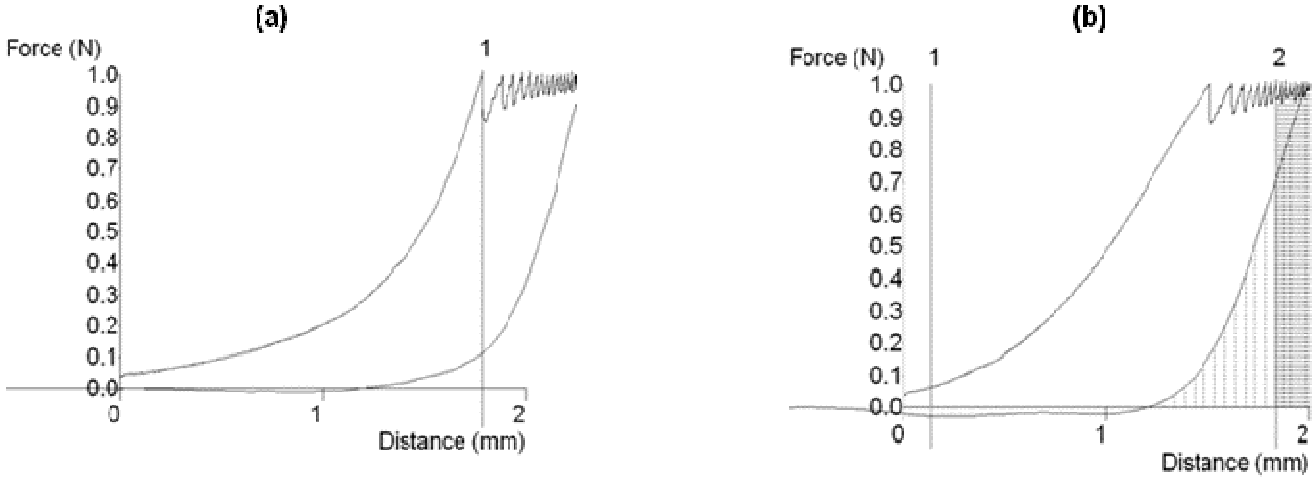

(Figure 2.1 (a) and (b)).

Figure 2.1: Typical force-distance curve of a pore-regulated matrix for determining both: (a) peak detachment force and (b) work of adhesion (N = 3 in all cases).

2.2.8. Matrix porosity analyses

2.2.8.1. Qualitative evaluation of matrix porosity

An inverse relationship exists between porosity and density with an elevation in density being an indication of low porosity (Dourdain, *et al*., 2006). The porosities (ø) of the matrices were computed from the true and apparent densities of the formulations using volume and weight measurements. The mathematical expression used is stated in Equation 2.4.

$$\text{Porosity} = \frac{\rho_{bulk} - \rho_{apparent}}{\rho_{bulk}} \times 100 \qquad \textit{(Equation 2.4)}$$

The bulk (ρ_{bulk}) and apparent ($\rho_{apparent}$) densities were calculated using the mass and volume measurements of the dry and hydrated matrices respectively. The weights and dimensions of the samples were recorded using a Mettler Toledo weighing balance (Microsep Pty Ltd, Switzerland) and a manually operated vernier caliper (25 × 0.01mm capacity) respectively. Also, the parameters for computing the bulk density were measured 30 minutes post hydration because it was observed that at this time point, all the formulations had attained a

constant weight increment and the process of matrix loss had not yet commenced. All measurements were performed in triplicate.

2.2.8.2. Quantitative porosimetric analysis

Porosimetry is an analytical technique used to determine various quantifiable aspects of a material's porous nature such as cumulative pore volume, cumulative surface area, average pore diameter which provides information about pore types. In this regard, the average pore diameter ($þ_D$), cumulative pore volume ($þ_V$) and cumulative surface area of pores ($þ_{SA}$) were determined in triplicate using the surface area and porosity analyzer equipped with the ASAP 2020 V3.01 software (Micromeritics, ASAP 2020, Norcross, GA, USA). The computational algorithm developed by Barrett, Joyner and Halenda (i.e. the BJH method) which is based on the Kelvin equation (Equation 2.5) was employed for these computations. Generally, the BJH method visualizes the incremental decomposition of an experimental isotherm starting at the highest relative pressure or pore size. The BJH method quantifies the total adsorptive process which comprises of the pore-emptying (desorption) and film-thinning (adsorption) processes per cycle or step (Webb and Orr, 1997).

$$\ln \frac{P}{P_0} = - \frac{2\gamma v \cos \theta}{RTr_m} \qquad \textit{(Equation 2.5)}$$

Where P = the critical condensation pressure, γ = liquid surface tension, v = molar volume of the condensed adsorptive, θ = contact angle between the solid and condensed phase (taken to be zero when adsorptive gas is nitrogen, hence cos θ = 1), r_m = mean radius of curvature of the liquid meniscus, P/P_0 = relative pressure, R = universal gas pressure and T = absolute temperature.

For this analysis, a dry sample weight of 130±10mg was employed for all 15 formulations. The porosimetric investigations were conducted in two phases, degassing and analysis stages. Samples were subjected to degassing to remove air, gases and other adsorbed atmospheric vapor and species from the sample surface by employing specific heating gradients. The operating settings employed included temperature ramp rate (10°C/min), target temperature (30°C), evacuation rate (50mmHg/s), unrestricted evacuation (30mmHg), vacuum set point (500μmHg), evacuation time (60 minutes), heating hold temperature (35°C), hold time (900 minutes), evacuation and heating hold pressure (100mmHg) and analysis time (400 minutes).

2.2.9. Surface morphological characterization of the P-RPMs

The nature and architecture of the porous surface morphology of each formulation was viewed and characterized using Scanning Electron Microscopy (SEM). Samples (8mm diameter × 4mm thickness) were sputter-coated with gold-palladium and viewed four times from different angles under a JSM-840 Scanning Electron Microscope (JEOL 840, Tokyo, Japan) at a voltage of 20 keV and a magnification of 1000×.

2.2.10. Rheological investigations of the homogenous co-particulate blends

The rheological characteristics in terms of viscosity (η) and deformation (γ) of the un-lyophilized homogenous blends used in preparing the porous matrices and their overall influence on the matrix integrity was investigated using the Modular Advanced Rheometer System equipped with the Haake Rheowin software (ThermoHaake MARS, Thermo Fischer Scientific, Karlsuhe, Germany). The rheometer stage was filled with 1mL of homogenous blend for each formulation. The rotor C35/1° Titan sensor type was employed. Rheological measurement parameters were fixed at an operational temperature of 25°C, analytical contact time of 180s, controlled rate ranging between 0 to $5s^{-1}$ and constant shear rate of 0 to $500s^{-1}$. Mean viscosity (η) and deformation (γ) values were computed at an average, constant shear rate of $250s^{-1}$. All determinations were done in triplicate.

2.2.11. Measurement of the physicomechanical strength of the P-RPMs

Textural analysis was used to evaluate the physicomechanical characteristics of the P-RPMs by determining relevant parameters. These included matrix resilience (M_R), energy of matrix distortion (ϵ_D) and matrix firmness (M_F). These physicomechanical parameters were selected for evaluation because of their prominent and direct effect on matrix integrity, degree of entanglement and disentanglement of the polymeric chain and drug release modulation (Pillay and Danckwerts, 2002; Kolawole *et al*., 2007). A calibrated TA.*XTplus* Texture Analyzer (Stable Micro Systems, Surrey, England) fitted with a cylindrical steel probe (50mm diameter) was employed for the determination of the matrix resilience while the energy of matrix distortion and matrix firmness were measured using a flat-tipped steel probe (2mm diameter). For all determinations, the textural settings listed in Table 2.4 were fixed throughout. Data was captured at a rate of 200 points per second via Texture Exponent Software (Version 3.2) and all determinations were done in triplicate. Typical force-distance and force-time profiles generated for computation of the textural parameters are shown in Figure 2.2. Figure 2.2a depicts a typical force-distance profile for computing the matrix

firmness (N/mm) and energy of matrix distortion (J). Matrix firmness is provided by the gradient between the initial force (anchor 1) and the maximum force attained (anchor 2) while the energy of matrix distortion is calculated as the area under the curve (AUC) of a force-distance profile. Figure 2.2b depicts a typical force-time profile used to calculate the matrix resilience which is represented by the percentage of the ratio between the AUC of anchors 2 and 3 ($AUC_{2,3}$) and anchors 1 and 2 ($AUC_{1,2}$).

Table 2.4: Textural settings employed for the determination of matrix resilience, energy of matrix distortion and matrix firmness

	Settings		
Parameters	**M_R (%) [a]**	**M_F (N/mm) [b]**	**ϵ_D (J)[c]**
Pre-test speed	1mm/sec	1mm/sec	1mm/sec
Test speed	0.5mm/sec	0.5mm/sec	0.5mm/sec
Post-test speed	10mm/sec	10mm/sec	10mm/sec
Compression force	-	40N	40N
Trigger type	Auto	Auto	Auto
Trigger force	0.5N	0.5N	0.5N
Load cell	5kg	5kg	5kg
Compression strain	50%	-	-

[a] Matrix resilience; [b] Matrix firmness; [c] Energy of matrix deformation

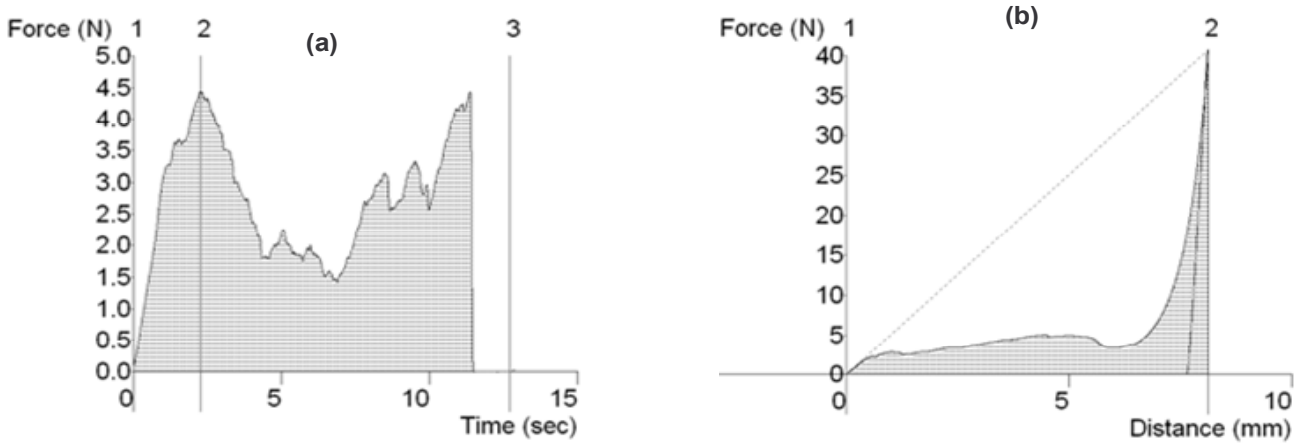

Figure 2.2: Typical force-distance and force-time profiles of the P-RPM formulation for determining (a) matrix firmness and energy of matrix distortion and (b) matrix resilience (N=3 in all cases).

2.2.12. Preparation of calibration curves for PS in simulated saliva (pH 6.8) and simulated plasma (pH 7.4)

Stock solutions were prepared by separately dissolving 10mg of PS in 100mL of simulated saliva (pH 6.8) and simulated plasma (pH 7.4). From the stock, a series of dilute standard solutions of the following concentrations: 0.01, 0.03, 0.04, and 0.06 mg/mL were prepared. The absorbance of each standard solution was determined at the maximum wavelength (λ_{max}) of 206nm for PS and fitted into the linear polynomial equations (*simulated saliva: y=16.516x; R^2=0.995 and simulated plasma: y=17.004x; R^2=0.997*). Subsequently, linear calibration curves for PS in simulated saliva and plasma were constructed respectively (Figures 2.3 (a) and (b)).

2.2.13. Constrained statistical optimization

The primary aim of this statistical process was to develop an optimal pore-regulated matrix for transbuccal drug delivery applications to provide sustained systemic release. After generating the quadratic polynomial regressions from the Box-Behnken design template which related the independent to the dependent variables, experimental results were fitted within set constraints for predicting the optimal formulation.

A simultaneous optimization approach was performed using a Response Surface Optimizer (Minitab software, Version 14, USA). With this technique, constraints were set to obtain levels of independent variables that will simultaneously manipulate the relevant response parameters or dependent variables to the desired statistically optimal levels. Consequently, a target level was set for the mean dissolution time (indicative of drug release behaviour) while the drug loading capacity, bio-adhesion, and cumulative drug permeation were maximized with respect to the desired release behaviour. With regards to the purpose of this constrained optimization process, the response parameters, mean dissolution time, drug loading capacity, bio-adhesion, and cumulative drug permeation, were set at different levels (Table 2.5).

The abovementioned response parameters were selected for optimization purposes as they are a function of all measured physicochemical and physicomechanical parameters which have been noted to influence the overall performance of the P-RPM to suit its intended application as a transbuccal drug delivery system. A desirability function, a value that

measures the accuracy of the statistical process, closest to one (0.96) which is indicative of the accuracy and efficiency of the statistical optimizer was obtained.

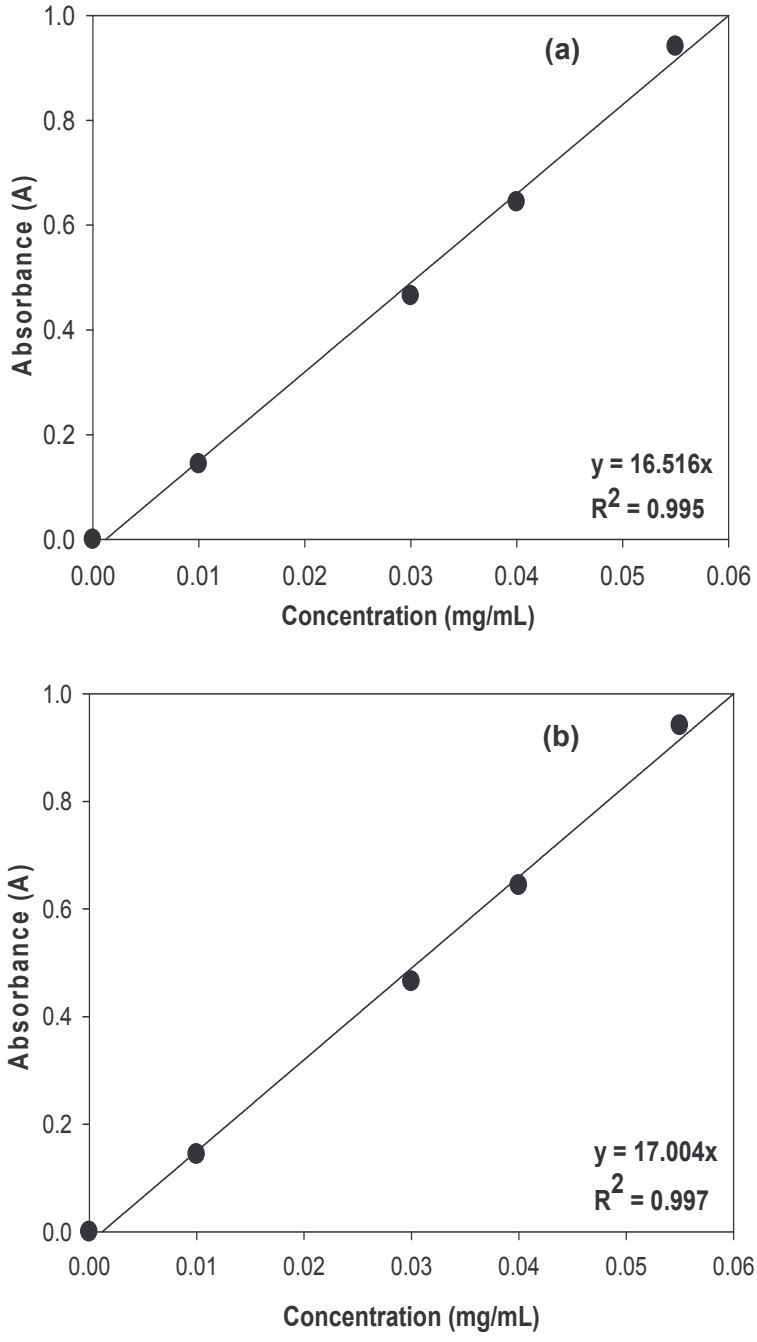

Figure 2.3: Calibration curves of PS in (a) simulated saliva (pH 6.8) and (b) simulated plasma (pH 7.4) at 206nm (N=3 and Standard Deviation ≤ 0.05 in all cases).

Table 2.5: Numerical targets set for the selected response parameters

Parameters	Statistical Goal	Lower	Upper	Optimization Goal
Mean dissolution time (MDT) (Minutes)	Target	80.00	100.00	90.00
Drug loading capacity (DLC) (%)	Maximum	90.00	100.00	100.00
Bioadhesive Strength (BA) (Newton)	Maximum	1.10	1.20	1.20
Cumulative drug permeation (PA) (%)	Maximum	80.00	90.00	90.00

A one-way analysis of variance (ANOVA) was applied to estimate the significance and reliability of the statistical model. The response parameters employed above were also chosen for the simultaneous optimization process because of the correlation measures that were employed to estimate the fitness of the statistical model for accurate prediction. The model-dependent terms employed in this study included the: (i) *p-values* set at 95% confidence level ($p < 0.05$ were considered as statistically significant) and (ii) the correlation coefficient, R^2 (set at values >0.90 because of the complexities of the quadratic experimental design approach). Table 2.6 outlines the levels of significance for the response parameters.

Table 2.6: Levels of statistical significance of the response parameters employing ANOVA

Response Parameters	*p-values*	R^2
Mean dissolution time	0.031	0.907
Drug loading capacity	0.013	0.948
Bioadhesive strength	0.048	0.905
Cumulative drug permeation	0.011	0.991

2.2.14. Evaluation of the impact of pore-regulation on relevant physical quantities using a mathematical approach

The influence of pore-regulation on the magnitude of specific quantifiable physical properties which are paramount to the performance of the P-RPM as a transbuccal drug delivery system was also evaluated. In this regard, the values obtained for the average pore diameter (ρ_D) and cumulative surface area of pores (ρ_{SA}) were selected as measures for pore-regulation. Besides, the physical quantities selected for evaluation included drug release measured as the mean dissolution time, *ex vivo* drug permeation, peak force of detachment which is a measure of bioadhesion, viscosity, drug loading capacity and matrix resilience which is a measure of physicomechanical strength. A polynomial mathematical

expression was employed to visualize the existing trends/relationships by assessing the linearity/non-linearity of graphical outputs which were validated with the correlation coefficient, R^2. The Sigma Plot, Version 11 software (Systat Software Inc. California, USA) was employed for this purpose.

2.3. RESULTS AND DISCUSSION

2.3.1. Physical appearance and weight variability

Generally, the pore-regulated matrices appeared as whitish, compact, semi-circular platforms with a diameter of 8mm and thickness of 4mm. Also, the matrices presented with convex-shaped base and a flat surface which can enhance its fitting unto the curved inner surface of the cheek (buccal mucosa) which may augment unidirectional drug release through the mucosa and prevent loss of drug due to washout with saliva. A digital photograph of a typical pore-regulated matrix is shown in Figure 2.4.

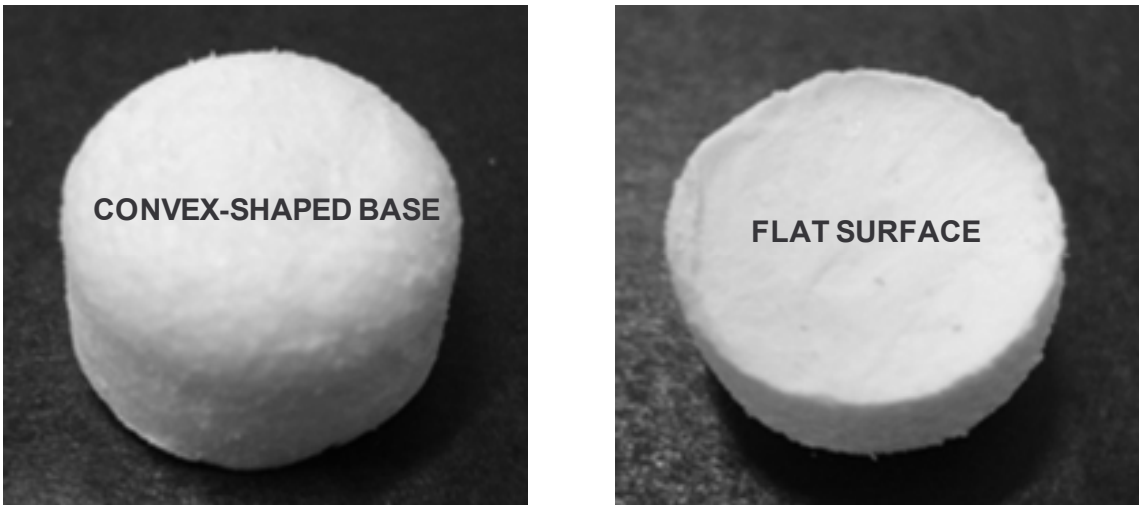

Figure 2.4: Typical digital photographs of pore regulated matrices with convex-shaped base and flat surface.

Overall the matrices had weights ranging from lowest (121.95±0.95 mg) to highest (133.75±0.35 mg) and an average weight of 128.44±3.49 mg for all the 15 formulations. The minimal differences (correlation factor, r = 0.459) in weights exhibited by the 15 formulations may be attributable to the differences in the quantities of the components (both solute and

solvent levels) employed in the fabrication of each set of formulation. This possibly has an influence on the porous network of each set of matrix formulation due to the presence of characteristic air pockets, pore geometries and interconnectors. As regards intra-formulation weight differences, a close relationship (correlation factor, r = 0.961) existed amongst each set of matrices prepared from the same formulation composition. Consequently, it can be proposed that the interphase, co-particulate, co-solvent, homogenization technique coupled with pre-freezing and lyophilization utilized in preparing these porous matrices was efficient and produced a homogenous blend which minimized disparities within the same formulation batch. The average weights of the 15 formulations are presented in Figure 2.5.

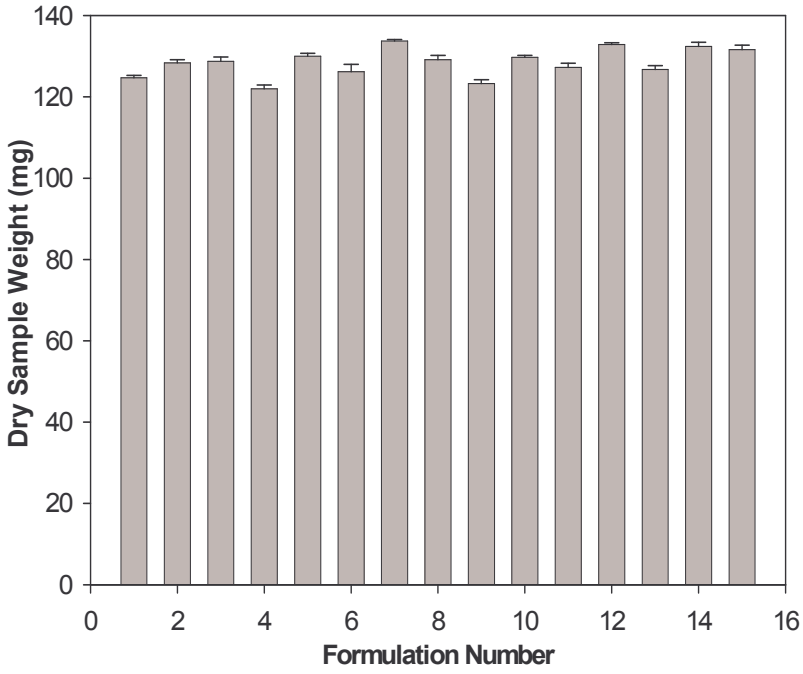

Figure 2.5: A representation of inter-formulation and intra-formulation weight variations and similarities respectively (N = 3, Standard Deviation ≤ 1.80 mg in all cases).

2.3.2. Drug release from the matrices

Diverse release patterns were observed for the 15 formulations which may be associated with the various degrees of co-particulate dispersion, interphase homogenization, solute-solvent interaction and lyophilization due to the differences in the quantities of the constituents utilized in fabricating each formulation (Table 2.3). Figure 2.6 illustrates the drug release trends exhibited by the 15 formulations. The varied dissolution patterns displayed by

the 15 formulations were analyzed and substantiated by the time-point approach referred to as mean dissolution time (MDT). The application of the MDT provides a more accurate view of the drug release behaviour as it is determined as the sum of the individual periods of time during which a specific fraction of the total drug dose is released (Pillay and Fassihi, 1998; Rinaki *et al*., 2003). Equation 2.6 was employed in the calculation of the MDT.

$$MDT = \sum_{i=1}^{n} t_i \frac{M_t}{M_\infty} \qquad \textit{(Equation 2.6)}$$

Where M_t is the fraction of dose released in time t_i, t_i = ½ (t_i + t_{i-1}) and M_∞ corresponds to the loading dose.

The $MDT_{50\%}$ data point was selected for the 15 formulations as this was applicable to all generated profiles (Figure 2.6). The $MDT_{50\%}$ numerical values are presented in Table 2.7. Generally for this set of data, the $MDT_{50\%}$ values were categorized as low ($MDT_{50\%}$ < 110.00 minutes) and high ($MDT_{50\%}$ > 110.00 minutes) which represent rapid and prolonged/controlled drug release patterns respectively.

All the 15 formulations elicited a low level of burst release of drug at t_{30min} and this may be attributable to their porous nature (Figure 2.6). This initial relatively quick liberation of drug molecules was followed by a moderately consistent release trend over time. The observed pattern may be of advantage to the intended application of this drug delivery system as the initial burst release might initiate the pharmacological action which is sustained by the consistent release of drug molecules over time. The P-RPMs demonstrated the potential for application as a controlled release system over 8 hours. The levels of both hydrophilic and hydrophobic co-particulate component contained in each formulation appeared to have noticeable complex effects on the drug release pattern. Generally, formulations that comprised of higher levels of hydrophobic solutes than the hydrophilic components displayed more controlled release patterns while those containing higher levels of the hydrophilic components relative to the hydrophobic solutes showed less controlled drug release behaviours.

Table 2.7: $MDT_{50\%}$ values depicting the drug release characteristics of the 15 formulations

Formulation	$MDT_{50\%}$ (minutes)
1	104.00
2	85.00
3	98.00
4	105.00
5	104.50
6	220.00
7	225.00
8	88.50
9	15.00
10	185.00
11	100.00
12	210.00
13	90.00
14	161.00
15	22.50

Standard Deviation ≤ 5.08 minutes in all cases

Furthermore, the quantities of the pore-forming agents, water and ethanol, appeared to influence drug release behaviour of the formulations. This may be attributable to the susceptibility of the frozen, solidified (due to the pre-freezing of the homogenous blend) individual pore-forming agent to sublimation during the process of lyophilization due to the differences in their individual boiling points (ethanol = 78.3°C and water = 100.0°C). Consequently, ethanol which has a lower boiling point than water may be converted to gas more quickly during the process of lyophilization thereby forming a more open porous network as compared to water, its higher boiling point counterpart producing a more closely knitted porous structure. Overall, the differences in their pore-forming capacities can influence the processes of water influx, hydration and matrix disentangling which may then influence the exhibited drug release behaviour of each formulation.

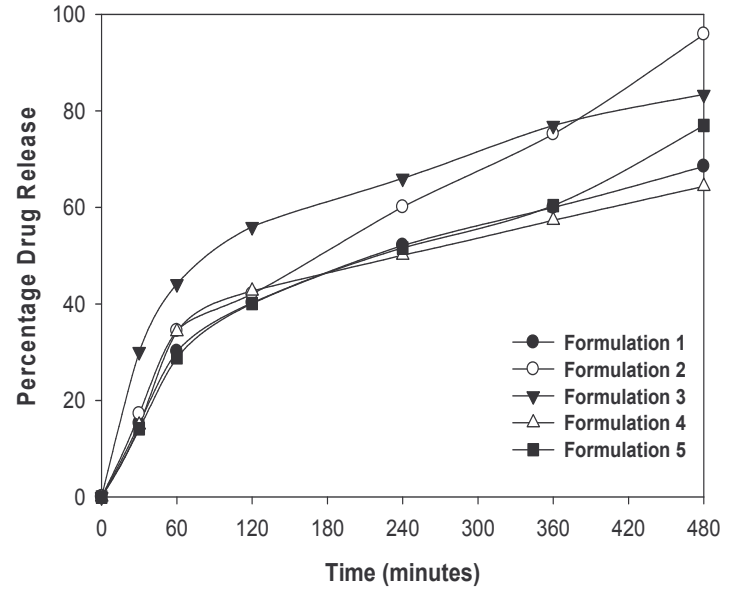

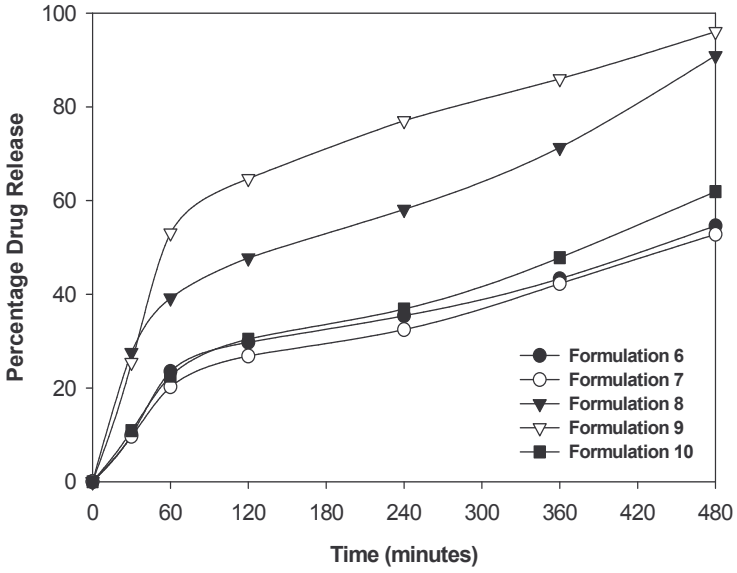

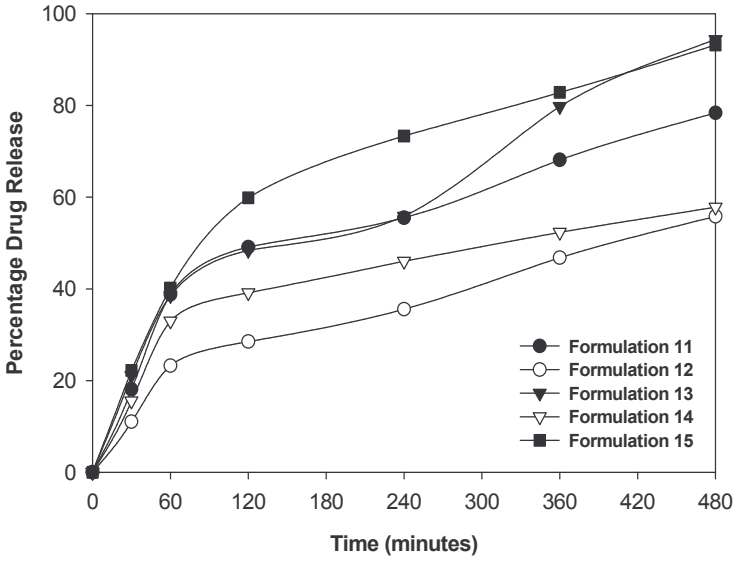

Figure 2.6: Drug release profiles for the 15 formulations in simulated saliva (pH 6.8) prior to optimization (N=3 and Standard Deviation ≤ 4.56% in all cases).

2.3.3. Drug loading capacity of the P-RPMs

Generally, effective drug loading was attained with values at 53.14 ± 2.19 to 99.02 ± 0.74% (Table 2.8). Drug loading does not appear to follow on any particular trend as regards the level of solute or solvent compositions for each formulation. Nevertheless, the quantity of PVA in the formulation appears to have significantly impacted drug loading with formulation 4 containing a higher quantity of PVA (800mg; Table 2.3) displaying a higher DLC (99.10 ± 0.49; Table 2.8) compared with formulation 13 containing 300mg PVA (Table 2.3) showing a lower DLC value (53.14 ± 2.55). Overall, it can be proposed that the extent of drug loading could be related to the degree of miscibility of the model drug molecules with the respective constituents of the homogenous blends.

Table 2.8: Percentage drug loading capacity for the 15 formulations

Formulation	%Drug Loading Capacity (DLC) ± SD*
1	58.60 ± 1.68
2	80.54 ± 0.33
3	95.14 ± 2.54
4	99.10 ± 0.49
5	94.64 ± 3.77
6	99.02 ± 0.21
7	97.54 ± 1.03
8	66.83 ± 2.24
9	83.27 ± 3.34
10	79.28 ± 2.27
11	94.85 ± 1.98
12	98.64 ± 0.88
13	53.14 ± 2.55
14	81.38 ± 1.67
15	79.18 ±1.09

SD - Standard Deviation

2.3.4. Extent of permeation of drug molecules through the porcine buccal mucosa

The capabilities of the formulations to initiate and sustain the permeation of PS molecules through the porcine buccal tissue was observed and results illustrated with Figures 2.7 and 2.8 as cumulative drug penetration (%) and drug flux ($mgcm^{-2}min^{-1}$) respectively over 8

hours for the 15 formulations. The drug flux values were calculated using Equation 2.2. Overall, the formulations showed diverse permeation-enhancing capabilities as different amounts of drug molecules passed through the tissue within the set experimentation time (Figure 2.7). The different levels of each permeation enhancer (span 80, chitosan and menthol) (Table 2.3) employed in the fabrication of the P-RPMs displayed extensive co-interactive, combined synergistic influences on each other but a relatively coherent general pattern of impact on permeation initiation and sustenance was noticed. Overall, the permeation enhancers were observed to be most efficient at mid to low factor levels while the converse is applicable to the highest factor levels of the enhancers.

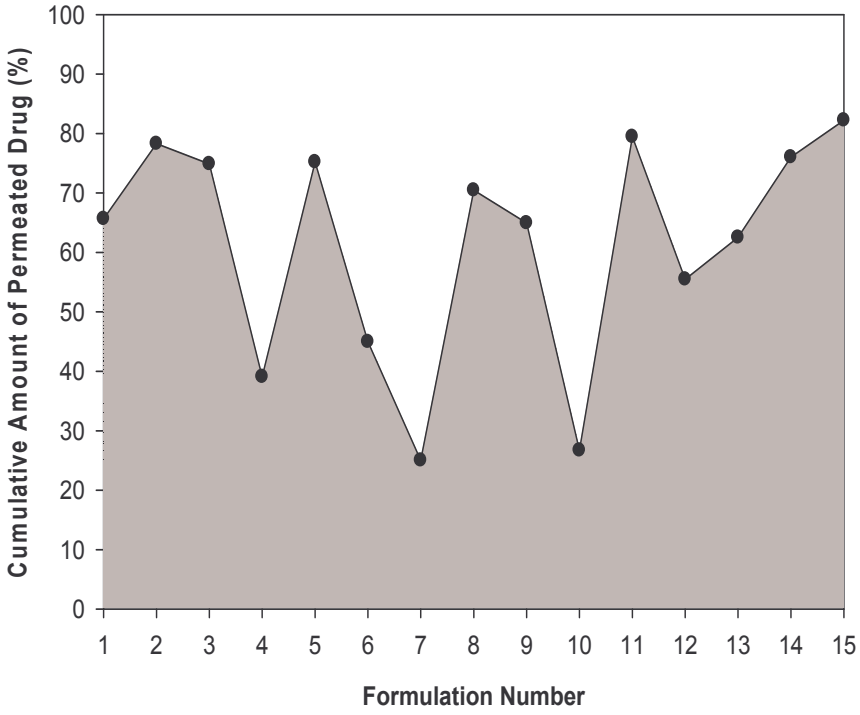

Figure 2.7: Cumulative quantity of PS that diffused through the porcine buccal mucosa into the receptor compartment in 8 hours (N = 3 and Standard Deviation ≤ 1.41 % in all cases).

The values of cumulative flux, the rate of drug permeation over the surface area, differ in the formulations, which may be due to synergistic or antagonistic interactions amongst the permeation enhancers as well as with other components within each P-RPM matrix. A linear relationship (R^2 = 0.89) was observed between the percentage quantity of drug that permeated through the tissue into the recipient compartment and the drug flux (Figure 2.9).

In other words, the rate at which the drug molecules permeate through the tissue (flux) was a determining factor for the amount of drug that would eventually be detectable in the recipient compartment or the quantity that permeated through the buccal mucosal specimen. Therefore, drug permeation was dependent on the flux relative to fixed surface area.

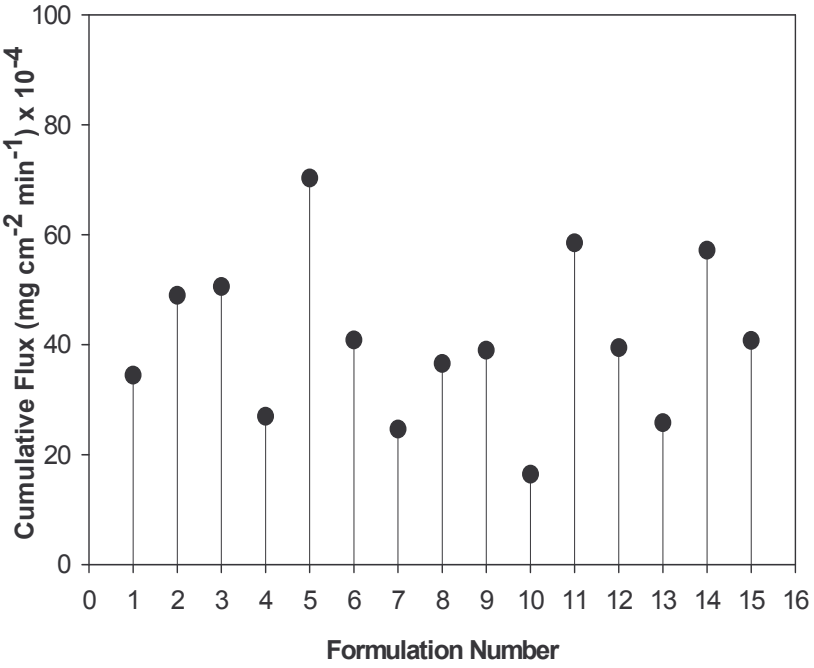

Figure 2.8: Cumulative steady state flux values computed over 8 hours for the 15 formulations (N = 3 and Standard Deviation ≤ 1.99×10^{-4} mg cm^{-2} min^{-1} in all cases).

The permeability coefficient which is a measure of the distance traveled by the drug molecules per minute varied for each formulation (Figure 2.10). Alternatively, the permeability coefficient may be described as the velocity of drug diffusion through the tissue based on its mathematical unit (Equation 2.3). The differences observed in the values obtained for each formulation may be indicative of the fact that the rate at which drug permeates the tissue specimens may be dependent on amount of drug in the donor compartment, the composition of each matrix (in terms of the ratios of the independent variables that make up each matrix) as well as the drug flux.

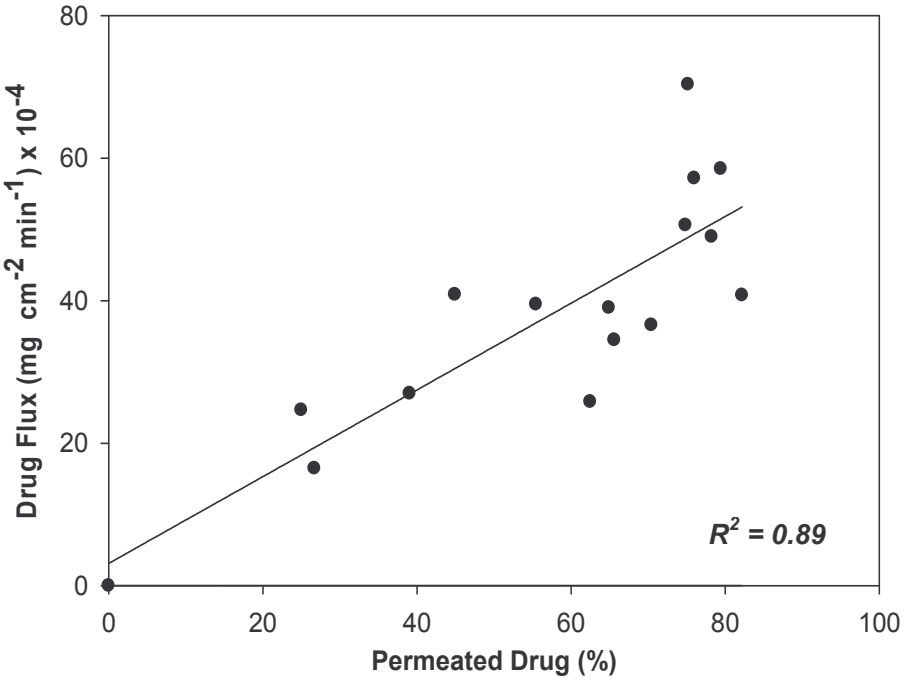

Figure 2.9: Linear relationship between the percentage amount of permeated drug and flux.

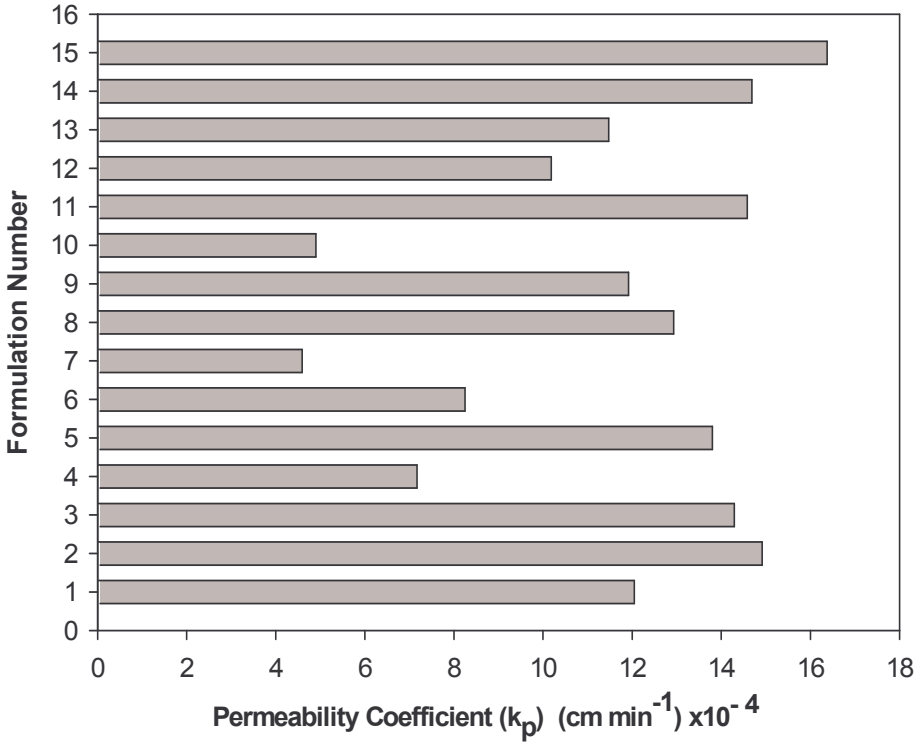

Figure 2.10: Depiction of the permeability coefficient values for the 15 formulations (N=3 and Standard Deviation ≤ 1.02×10^{-4}cm min^{-1} in all cases).

2.3.5. *Ex vivo* bioadhesion testing

The capability of the formulations to adhere to the model buccal mucosal tissue was made evident by the values obtained for the peak force of detachment (F_{det}) (0.9636 ± 0.015 to 1.042 ± 0.025 N) and work of adhesion (w_{adh}) (0.0014 ± 0.00005 to 0.0028 ± 0.00008 J) (Figure 2.11 (a) and (b)). No specific trend was observed with the differences in the quantities of the bioadhesive components (Gelatin and Carbopol 974) included during the preparation of each formulation. It can be proposed that gelatin and carbopol 974 complemented each other in influencing the overall bioadhesive strength of the porous matrices. This explains why all the formulations showed a sizeable degree of bioadhesive competence. Additionally, particular patterns directly or inversely relating F_{det} to w_{adh} were absent implying that the F_{det} did not specifically influence the values of w_{adh}. This may be attributable to the fact that the energy expended during the process of bioadhesion or the force of detachment are extensively influenced by the inter-surface electrostatic interactions between the different matrices, buccal mucosal tissue, and simulated saliva that may be dependent on the proportions of the bioadhesive agents as well as other compounds present within each matrix.

2.3.6. Measurement of matrix porosity

2.3.6.1. Qualitative measurement of matrix porosity

The outcome of this study showed that all the formulations are porous with values ranging from 74.928 to 86.116 % (Figure 2.12). With pores being the void spaces within the matrix, porosity in this case measures the influx of water molecules into the matrix to fill the empty spaces or pores. Consequently, an increase in the numerical value of qualitative porosity values should result in a more porous matrix and vice versa (Figure 2.12).

To further evaluate the impact of the varying of porosity values obtained for each formulation, a comparison was made with their drug release and surface morphological characteristics. Generally, formulations with lower porosity values, ≤ 79.90 %, (formulations 1, 6, 7, 12 and 14) displayed slower release rates when compared with those with higher porosity values, > 80.490 %, (formulations 2, 8, 9 and 10) showed faster drug release behaviour (Figures 2.6 and 2.12). Some exclusion to this observations included formulations 3, 5 11, 13 and 15 with lower, and formulation 4 with higher porosity values but demonstrated faster and slower release rates respectively. This overturn in drug release behaviour in relation to porosity

could be as a result of the influence of the pore interconnectors existing within each matrix. Therefore, it can be hypothesized that in addition to the pore structures, the nature of the pore interconnectors can also influence the influx of water molecules, the processes of hydration and loosening of the matrices which may subsequently affect the qualitative matrix porosity values and drug release in diverse ways.

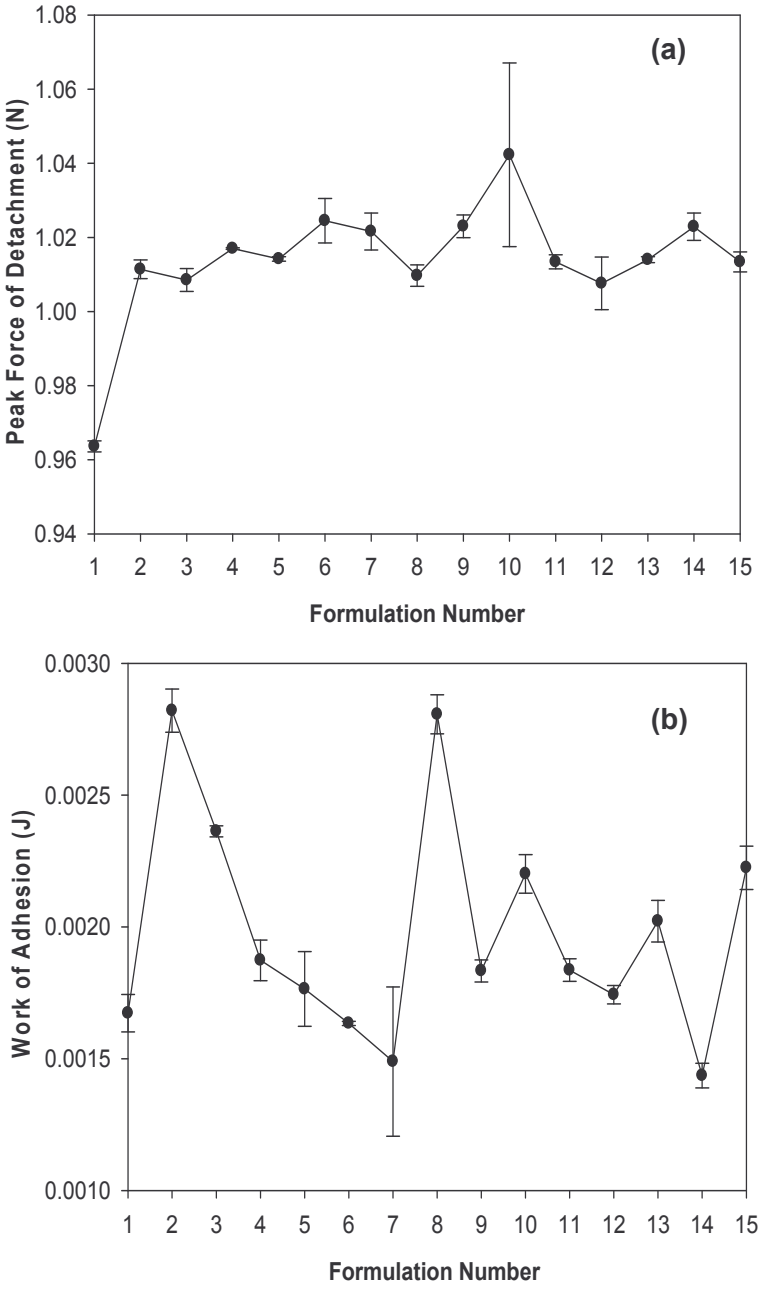

Figure 2.11: Numerical values of: (a) Peak detachment force in Newton and (b) Work or energy of bioadhesion in Joules of the 15 formulations (N = 3 and in all cases).

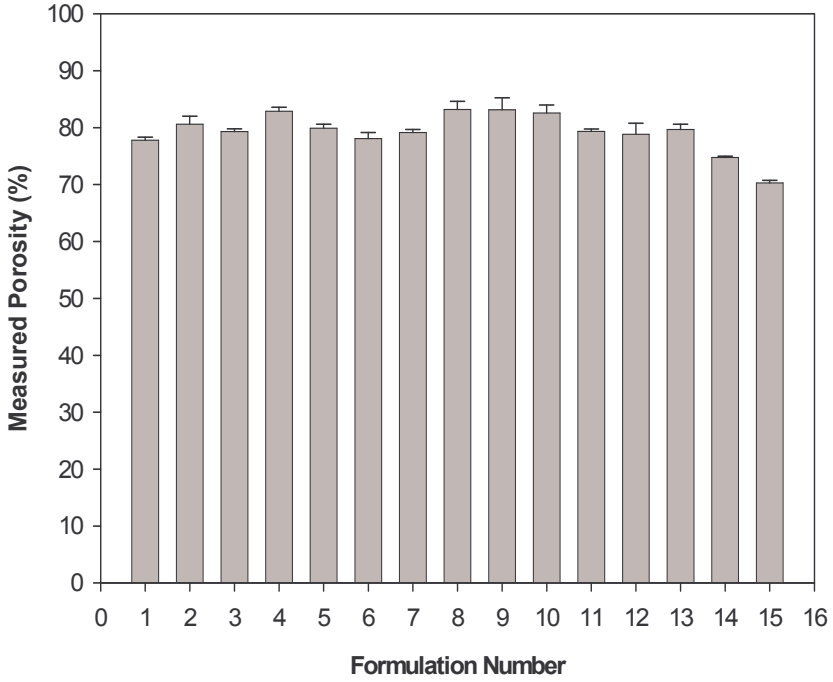

Figure 2.12: Qualitative measurement of porosity for the P-RPMs (N = 3 and in all cases).

2.3.6.2. Quantitative porosimetric analysis of the matrices

Porosimetric analysis quantified the cumulative pore volume, cumulative surface area, and average pore diameter. This investigation further validated the findings of the qualitative porosity measurement (Figure 2.12). Typical porosimetric profiles used in computing the abovementioned parameters are illustrated with Figure 2.13 (a), (b), (c) and (d). These profiles show that there is a close relationship between the processes of adsorption and desorption of nitrogen gas molecules to the surface of the pore structures which consist of the fundamental part of the accurate categorization of the pores with the matrix. Average pore diameter ranged between 40 and 100 Å, cumulative pore volume had values from 6.5×10^{-4} cm^3/g-$5\times10^{-3}cm^3/g$ and the cumulative surface area, as a measure of pore distribution, spanned over 28-800 cm^2/g. The abovementioned numerical measures demonstrated that the performance of the P-RPMs is highly dependent on the pore structure, diameter, pore distribution which also signifies the integrity and configuration of the interconnectors as well as the surface area of the porous matrix. These parameters vary for each formulation and were observed to have significant impact on their displayed physicochemical and physicomechanical properties. In addition, the range of pore sizes (40 Å - 100 Å) indicated that the 15 formulations were mesoporous in nature (20Å - 500Å; Webb and Orr, 1997). The numerical values for the average pore diameter, cumulative pore volume and surface area measured for the 15 experimental design formulations are outlined in Table 2.9.

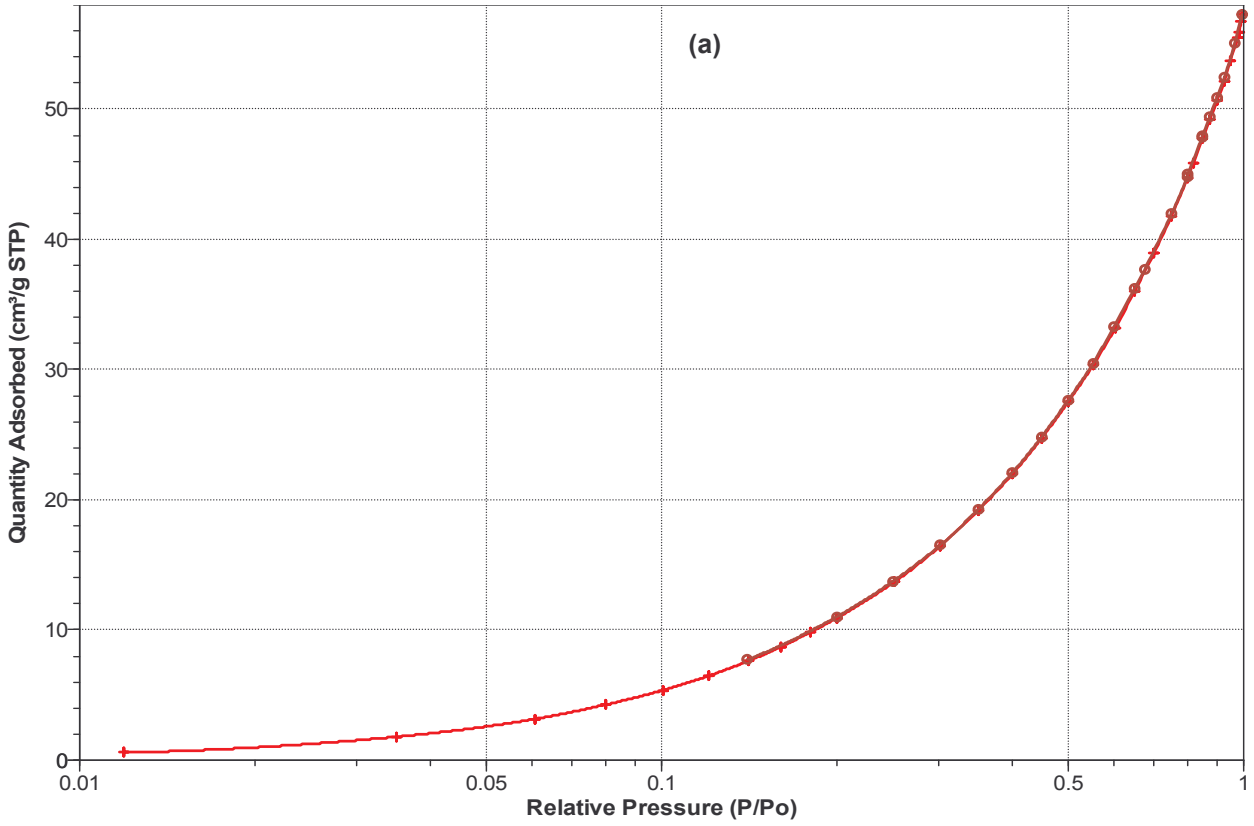
(a)
Quantity Adsorbed (cm³/g STP)
0
10
20
30
40
50
0.01
0.05
0.1
0.5
1
Relative Pressure (P/Po)

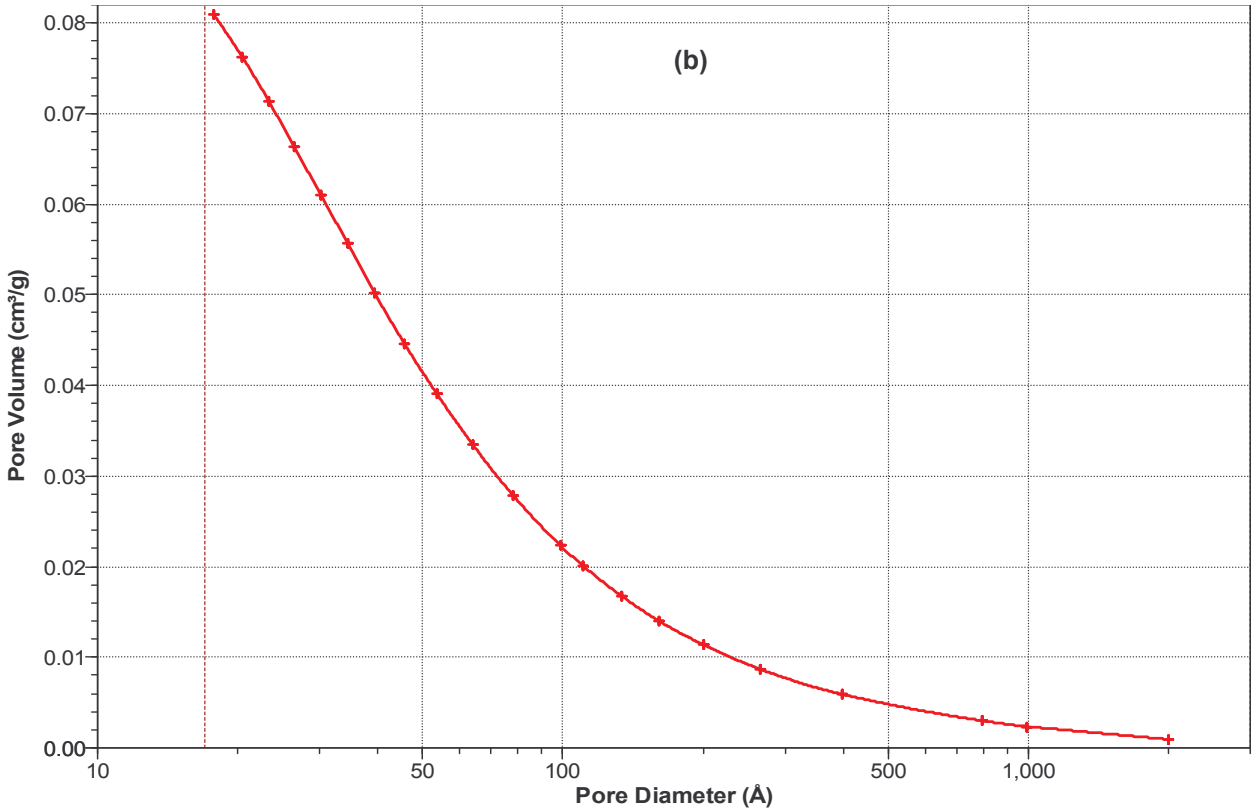
(b)
Pore Volume (cm³/g)
0.00
0.01
0.02
0.03
0.04
0.05
0.06
0.07
0.08
10
50
100
500
1,000
Pore Diameter (Å)

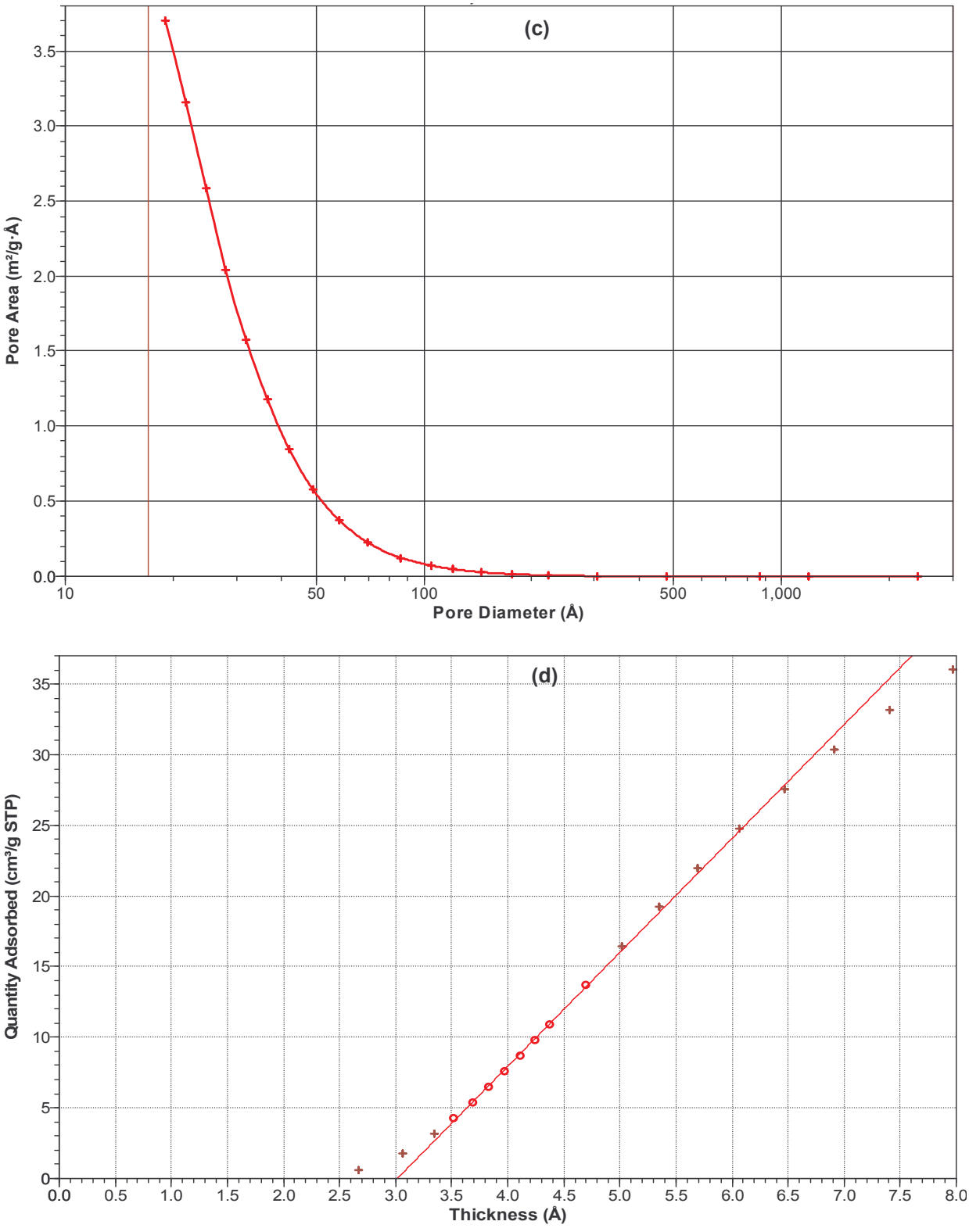

Figure 2.13: Typical porosimetric profiles showing the adsorption and desorption (a) isotherms, (b) BJH cumulative pore volume, (c) BJH cumulative pore surface area, (d) t-plot depicting the absence of micropores within the matrix (N = 3 and in all cases).

Table 2.9: The numerical values of the quantitative porosimetric measures

Formulation	$þ_D$ (Å) [a]	$Þ_V$ (cm^3/g) [b]	$þ_{SA}$ (cm^2/g) [c]
1	44.1411	0.0007	28.3800
2	71.5660	0.0044	245.7400
3	92.4072	0.0062	395.1500
4	45.2790	0.0081	714.6540
5	85.1234	0.0074	445.4750
6	79.4621	0.0037	213.3300
7	67.7782	0.0053	315.5400
8	62.7770	0.0062	396.5950
9	64.6940	0.0056	346.4700
10	74.4190	0.0045	244.6800
11	89.8222	0.0066	421.7950
12	70.7844	0.0041	236.6050
13	73.8142	0.0045	220.1500
14	48.4020	0.0071	590.4850
15	50.4130	0.0095	758.2450

[a] Average pore diameter (Standard Deviation ≤ 5Å in all cases), [b] Cumulative pore volume (Standard Deviation ≤ 7.74×10^{-4} cm^3/g in all cases), [c] Cumulative surface area of pores(Standard Deviation ≤ 20.97 cm^2/g in all cases). (N = 3 in all cases)

2.3.7. Examination of the surface morphologies of the P-RPMs

Scanning electron microscopy revealed the varieties of pore structures, distributions and interconnectors embedded within the sets of P-RPM matrices. Their surface porous configuration was rather complex, irregular and extensive. Typical surface morphologies are illustrated with Figure 2.14 below. Generally, the kinds of pore structures observed ranged from relatively circular (Figure 2.14 (a) and (b)) to those with asymmetrical geometries (Figure 2.14 (c) and (d)). The pores were comparatively widespread through the surfaces of each matrix. The interconnectors, which can be described as barriers or partitions that

demarcate the pores, were rather uneven and were described as either rigid (Figure 2.14 (e) and (f)), web-like/thread-like (Figure 2.14 (g) and (h)) or spongy (Figure 2.14 (i)) in structure.

A relationship between the surface morphology and drug release characteristics of the matrices was observed. It was noted that the pore interconnectors played a noticeable role in their drug release performances. Matrices with web-like, thread-like and spongy interconnectors (Figures 2.14 (g), (h), and (i) representing formulations 1, 2, 3, 4, 5, 8, 9, 11, 13 and 15 demonstrated quicker but controlled release rates with over 65% drug released within 8 hours (Figure 2.6). The converse was observed with formulations that showed rigid interconnectors (Figure 2.14 (e) and (f) representing formulations 6, 7, 10 and 14 in which case drug release was slower with less than 65% liberated over 8 hours (Figure 2.14). Consequently, a hypothesis that the pore interconnectors, in addition to the hole structures (pores), function as barriers within these porous matrices and play the role of regulating matrix hydration, disentanglement, diffusion of drug and erosion can be put forward.

The quantity of pore-forming agent added when preparing the matrices was noted to have had a significant influence on the exhibited porous structures of the matrices. In addition, ethanol presents to be a more potent pore forming agent than water with respect to this study as slight increment in the volume of ethanol resulted in visible changes in pore structure (i.e. enhanced porosity). For instance, formulations 2, 3, 4, 5, 6, 8, 11, 13 and 15 containing highest levels of ethanol (11mL and 13mL) displayed larger and higher volume of pores in terms of distribution (Figure 2.14 (a), (b) (d) and (f)) when compared with formulations 7, 12 and 14 (Figure 2.14 (d) and (e)) with highest volume of water (30mL) giving rise to lower volumes of pores distribution. Also, formulations 1, 9 and 10 are exceptions to this trend and this may be due to other physicochemical influences of the co-particulate components on the sublimation of the frozen pore-forming agents from the matrices during the process of lyophilization. For instance, formulations 2, 3, 4, 5, 6, 8, 11, 13 and 15 containing highest levels of ethanol (11mL and 13mL) displayed larger and higher volume of pores (Figure 2.14 (a), (b) and (h)) when compared with formulations 7, 12 and 14 (Figure 2.14 (d) and (f)) with highest volume of water (30mL) giving rise to lower volumes of pores distribution. In addition, formulations 1, 9 and 10 are exceptions to this trend and this may be due to other physicochemical influences of the co-particulate components on the sublimation of the frozen pore-forming agents from the matrices during the process of lyophilization.

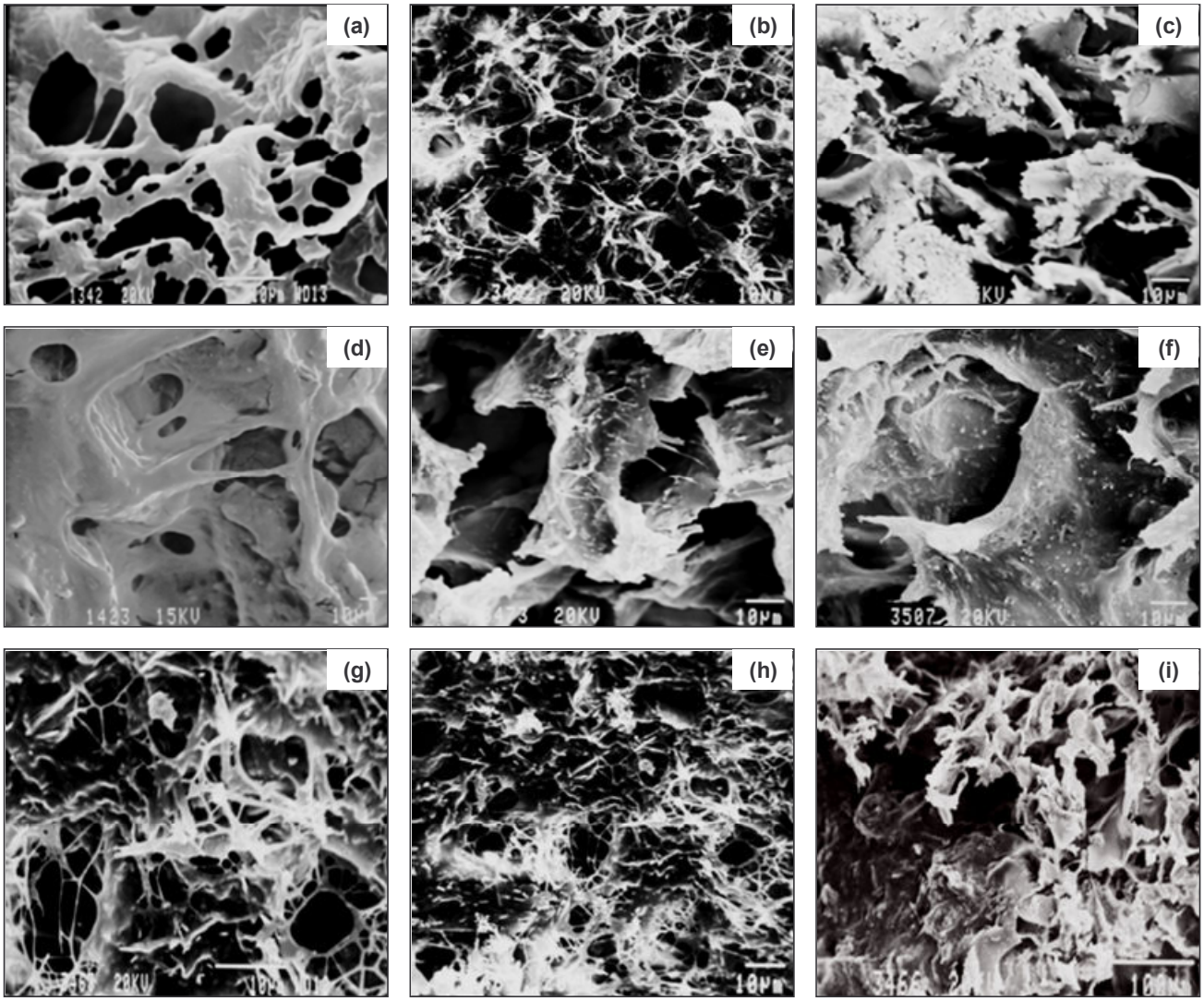

Figure 2.14: Typical scanning electron micrographs of the porous P-RPM matrices showing the diversity of their pore structures, distributions and interconnectors (magnification 1000×).

2.3.8. Elucidation of rheological behaviour of the homogenous co-particulate blends

Viscosity in this case can be described as a parameter that quantifies the resistance of the fluid co-particulate homogenous blends to flow with the application of an external compressive force. Generally, the behaviour of the prepared co-particulate homogenous blends for the 15 formulations can be described as non-Newtonian because their viscosities were dependent upon shear conditions (i.e. shear rate and shear stress). In other words, they cannot be described by a single constant viscosity as it changes with applied external force (shear stress and shear rate). For the blends therefore, an increase in shear stress and shear rate resulted in a decrease in viscosities. Figure 2.15 represents a typical profile

showing the relationship between viscosity, shear rate and shear stress for the homogenous blends.

The mean viscosity (η) computed at a constant shear rate for the 15 formulations differed with values ranging from ($0.7893\times10^4\pm0.0007$-$8.6580\times10^4\pm0.002$ Pa.s). The viscosities obtained were classified as low (<1.05×10^4 Pa.s), intermediate (>1.05×10^4 Pa.s but < 4×10^4 Pa.s) and high (>5×10^4 Pa.s but < 9×10^4 Pa.s) as this was the systematic approach employed for the interpretation of this set of data.

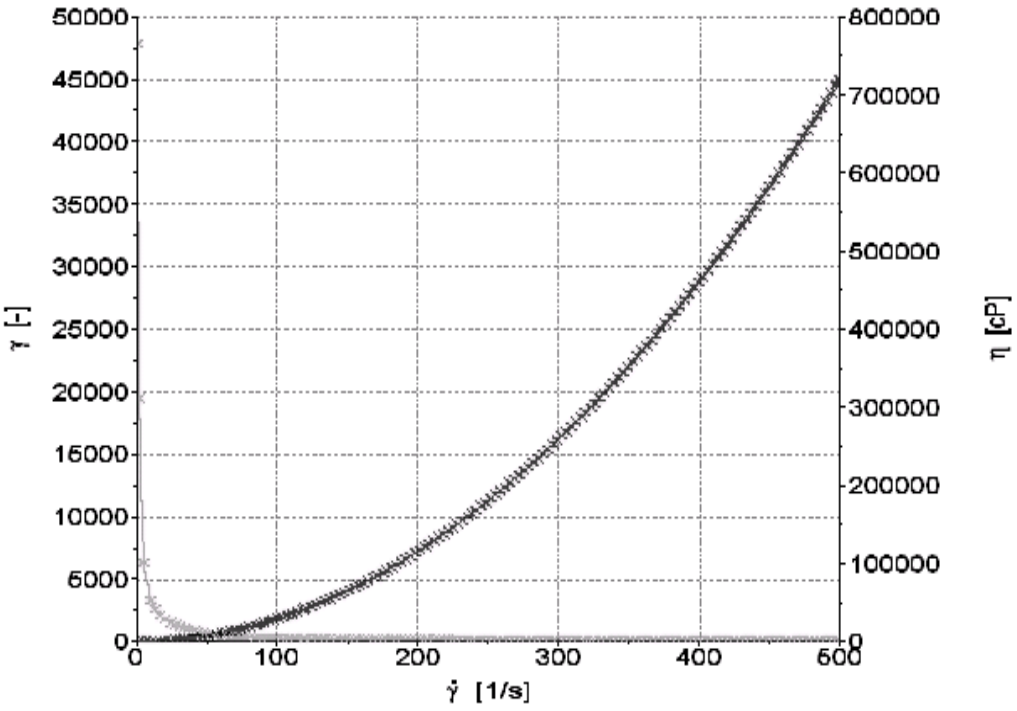

Figure 2.15: Typical profile showing the relationship between viscosity, shear stress and shear rate for the co-particulate homogenous blends (before lyophilization and freezing).

Comparing the viscosity with the surface morphology of the matrices, informing features were noted. The lowest range of viscosities (<1.05×10^4Pa.s) were recorded for formulations 1, 4 and 9 (Figure 2.14 (a), (d) and (i)) and they presented with irregular pore structures connected with spongy/fluffy barriers (interconnectors). Formulations 6, 7, 10 and 12 had the intermediate set of viscosity values (>1.05×10^4 Pa.s but < 4×10^4 Pa.s) and generally they displayed pore structures with asymmetrical dimensions and rigid/dense interconnectors

(Figures 2.14 (f), (g), (j) and (l)) with the exclusion of formulation 8 and 13. Formulations 2, 3, 5, 11, 14 and 15 generated the high viscosity magnitudes (>5×10^4 Pa.s but < 9×10^4 Pa.s) and their surfaces were characterized with circular/spherical pore structures with a high volume of distribution and web-like, low density interconnectors with the exception of formulation 14. An illustration of the different viscosity values are presented in Figure 2.16.

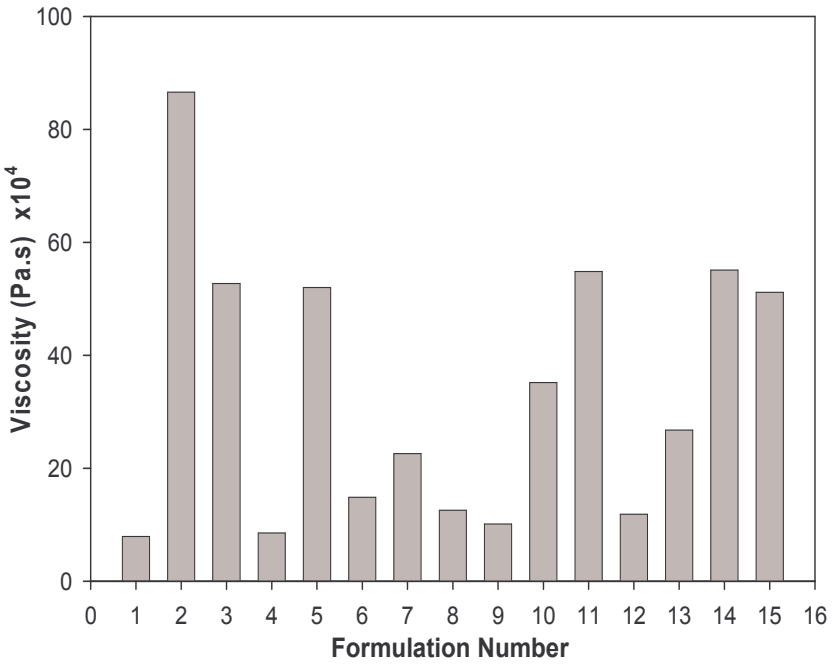

Figure 2.16: Ranges of mean viscosity values generated by the homogenous blends of the 15 formulations at a constant shear rate (N = 3 and Standard Deviation ≤ 0.002×10^4 Pa.s in all cases).

Overall, it can be proposed that viscosity (i.e. the degree of blend thickness) may possibly have an effect on the process of pre-freezing and sublimation of frozen, solidified solvent molecules to create the characteristic intra-matrix porous structure during lyophilization as both viscosity and freezing can be described as measures dependent on substance fluidity. The freezing (solidification) and subliming properties of the solvent molecules may be interfered with by the solute co-particulates present in the homogenous blend.

Deformation (ɣ) is described as a measure of change in internal structure of the homogenous blend due to an applied compressive external force. The homogenous blends for the 15

formulations displayed relatively constant deformation magnitudes ranging between 1.4880×10^4 and 1.5140×10^4 (Figure 2.17). The outcome of this test suggests that the blends are robust and stable to external force. Additionally, this may indicate the absence of irreversible, destructive chemical interactions or transformations amongst components during the processes of preparing the matrices. In other words, the method of preparing the matrices can be described as a physical interaction which does not irreversibly alter the chemical backbone structure of the components as well as their individual contributive properties which enhance the overall efficiency of the formulations to suit the intended application.

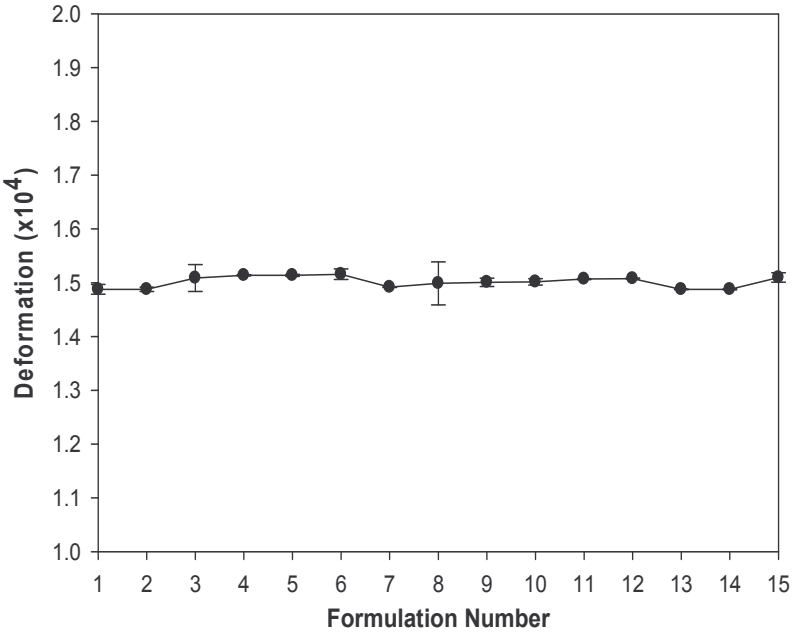

Figure 2.17: Deformation magnitudes of the homogenous blends of the 15 formulations at a constant shear rate (N = 3 in all cases).

2.3.9. Determination of physicomechanical parameters by textural analysis

The physicomechanical parameters measured for the 15 formulations were matrix resilience (M_R), energy of matrix distortion ($Є_D$) and the matrix firmness (M_F) (Table 2.10). The matrix resilience can be described as the elastic cohesiveness of the matrices that is the capability to recover to their original dimensions post the application of an external compressive strain. Matrix firmness is a measure of the force required to attain a given deformation of a body

while the energy of distortion is the work performed (or energy dissipated) in Joules to overcome the cohesive forces within the matrix. These parameters are measures of matrix integrity and robustness such that an elevated matrix resilience, firmness and reduced energy of distortion values indicate high matrix physicomechanical strength.

With respect to the outcome of this study, a direct relationship was observed between matrix resilience (M_R) and firmness (M_F) while an inverse association existed with the energy of matrix distortion ($Є_D$). In other words, an increase in resilience generated an increase in matrix firmness and a decrease in the energy of matrix distortion. Generally, formulations containing higher levels of the matrix stiffeners (polyvinyl alcohol, magnesium stearate and ethylcellulose) had elevated M_R and M_F and reduced $Є_D$ values while the converse was observed for formulation with low levels of the matrix stiffeners. The numerical values of physicomechanical parameters also show that the matrices have relatively low elasticity or recovery (from external stress) tendencies and resistance to deformation (Table 2.10) which may be due to their porous structure characterized by the presence of void spaces within the matrix.

2.3.10. Preparation and assessment of the optimized P-RPM formulation

Based on the statistical procedure employed, a formula was developed for the production of the optimized P-RPM (Table 2.11). The fabricated optimized P-RPM formulation was assessed to ascertain the existence of a correlation between the experimentally and fitted data as well as confirming the suitability of the experimental design employed. The formulation was assessed based on its drug loading capacity, bioadhesive strength, mean dissolution time and cumulative *ex vivo* drug permeation. Drug release and *ex vivo* permeation from this specialized matrix was targeted at 8 hours to aid convenience during use by the patient. The statistical significance measured as $p\text{-values} \leq 0.05$ and $R^2 > 0.90$ displayed (Table 2.6) by the response parameters indicate that the different levels of the independent formulation variables employed in constructing the optimized P-RPM had noticeable influence on its overall performance. A high degree of correlation between the experimental and statistically fitted values based on the ANOVA was observed for each selected response parameter (Table 2.12). This outcome further reveals the stability and adequacy of the statistical design employed for generating the desired optimized formulation.

Table 2.10: Matrix resilience, distortion and firmness numerical values for the P-RPMs

Formulation	[a]M_R (%)	[b]$Є_D$ (J)	[c]M_F (N/mm)
1	2.975	0.052	4.430
2	2.230	0.033	5.214
3	2.080	0.014	5.449
4	2.221	0.049	5.168
5	2.065	0.018	5.518
6	2.195	0.053	4.991
7	2.288	0.058	4.904
8	2.101	0.034	4.671
9	1.590	0.052	3.404
10	2.067	0.034	4.889
11	2.069	0.015	5.550
12	2.142	0.042	5.006
13	2.253	0.035	4.824
14	1.024	0.046	4.082
15	1.922	0.023	4.998

[a] Matrix resilience (Standard Deviation ≤ 0.407% in all cases), [b] Energy of matrix distortion (Standard Deviation ≤ 0.015J in all cases), [c] Matrix firmness (Standard Deviation ≤ 0.566N/mm in all cases). (N = 3 in all cases)

Table 2.11: Levels of solute and solvent components for the fabrication of the optimized P-RPM

Composition	Optimized Level
WCD [a]	[d] 0.00 mg/30 mL of water
ECD [b]	[e] 4.50 mg/9 mL of ethanol
SP 80 [c]	0.50 mL

[a] Water-based co-particulate dispersion; [b] Ethanol-based co-particulate dispersion; [c] Span 80

[d] 0 - PVA (800 mg) + HEC (350 mg) + GEL (400 mg) + CARB974 (100 mg) + DW (30 mL)
[e] 4.5 - CHTS (362.5 mg) + MS (312.5 mg) + MTH (275 mg) + ETH 10 (550 mg) +EtOH (9 mL)

Table 2.12: Comparison of the fitted and experimental values of the response parameter to assess the efficiency of the experimental design for formulation optimization

Response Parameters	Fitted Response	Experimental Response
Mean dissolution time (MDT) (minutes)	90.00	94.10 ± 2.90
Drug loading capacity (DLC) (%)	100.00	99.72 ± 3.56
Bioadhesive Strength (BA) (N)	1.20	1.18 ± 0.05
Cumulative drug permeation (PA) (%)	90.00	85.68 ± 3.33

2.3.11. Determination of the relationship between the parameters of pore-regulation and related physicochemical and physicomechanical properties

Generally, the direct and indirect mathematical linear fitting approach employed revealed the nature of relationship between the porosimetric measures employed (i.e. pore diameter and cumulative pore surface area) and the selected physicochemical and physicomechanical parameters. Figures 2.18 (a) - (f) and 2.19 (a) - (f) illustrate the graphical representations of the outcomes of this set of computations while the correlation coefficient, R^2 values, specified the type of relationship which exist between each set of parameter compared. In this regard, R^2 values < 0.5 indicate an indirect/inverse proportionality between the compared parameters while R^2 values > 0.5 signify a direct/dependent relationship between the evaluated parameters.

Overall, the porosimetric parameters, namely average pore diameter and cumulative pore surface area, influenced the magnitude of the investigated physicochemical and physicomechanical parameters either directly or indirectly. A direct relationship was observed between the average pore diameter and drug release measured as the mean dissolution time (R^2 = 0.861), cumulative *ex vivo* drug permeation (R^2 = 0.915), bioadhesion measured as the peak force of detachment (R^2 = 0.605), drug loading capacity (R^2 = 0.922) and blend viscosity (R^2 = 0.827) while an indirect/inverse relationship existed with the matrix resilience (R^2 = -0.692) (Figure 2.18). This indicates that the P-RPM formulation having relatively larger pore sizes can enhance transbuccal permeation of drug molecules, bioadhesion and drug loading while the homogenous blend employed in their preparation having higher viscosity possesses the potential of producing matrices with relatively larger pores. With drug release, it is observed that an increase in pore diameter results in an increase in the mean dissolution time which is indicative of prolonged drug release. This may actually show that the pores present within the P-RPM matrix possess unique capabilities of modulating the release of

drug molecules. With matrix resilience, an increase in pore diameter can decrease its magnitude or vice versa and can be associated with the presence of more air pockets within the matrix resulting in a reduction of the elasticity of the matrix on the application of an external force.

With the cumulative surface area of pores, a direct relationship was observed with the *ex vivo* drug permeation (R^2 = 0.716) and peak force of detachment (bioadhesion) (R^2 = 0.699) while an inverse proportionality was noted for mean dissolution time (R^2 = -0.511), drug loading capacity (R^2 = -0.541), matrix resilience (R^2 = -0.794) and viscosity (R^2 = -0.498) (Figure 2.19). In other words, the area within the matrix which is occupied by the pores is measured by the cumulative surface area. Therefore an increase in the surface area of pores results in a direct increase in the degree of drug permeation and bioadhesion to mucosal sites. On the contrary, a decline or elevation in the cumulative surface area occupied by the pore structures can result in a respective increase or decrease in the magnitude of mean dissolution time, drug loading capacity, matrix resilience and viscosity. Focusing on drug release measured as the mean dissolution time, it can be proposed that the release of drug molecules from the P-RPM formulations is not solely dependent on the pore diameter but also on the surface area of the pore. This explains why the trend observed for the comparison of pore surface area with the mean dissolution is opposite to the noted pattern for pore diameter. Thus, a higher surface area of pore structures will result in lower mean dissolution time values which are indicative of a rapid drug release pattern and vice versa. Furthermore, drug loading capacity appears to be more influenced by diameter of the pores than their surface area while with matrix resilience, the impacts of both pore diameter and surface area are similar. In addition, the viscosity of the co-particulate homogenous blend seems to impact the pore surface area than the pore diameter such that a decrease in blend viscosity generates a more porous matrix than its more viscous counterpart.

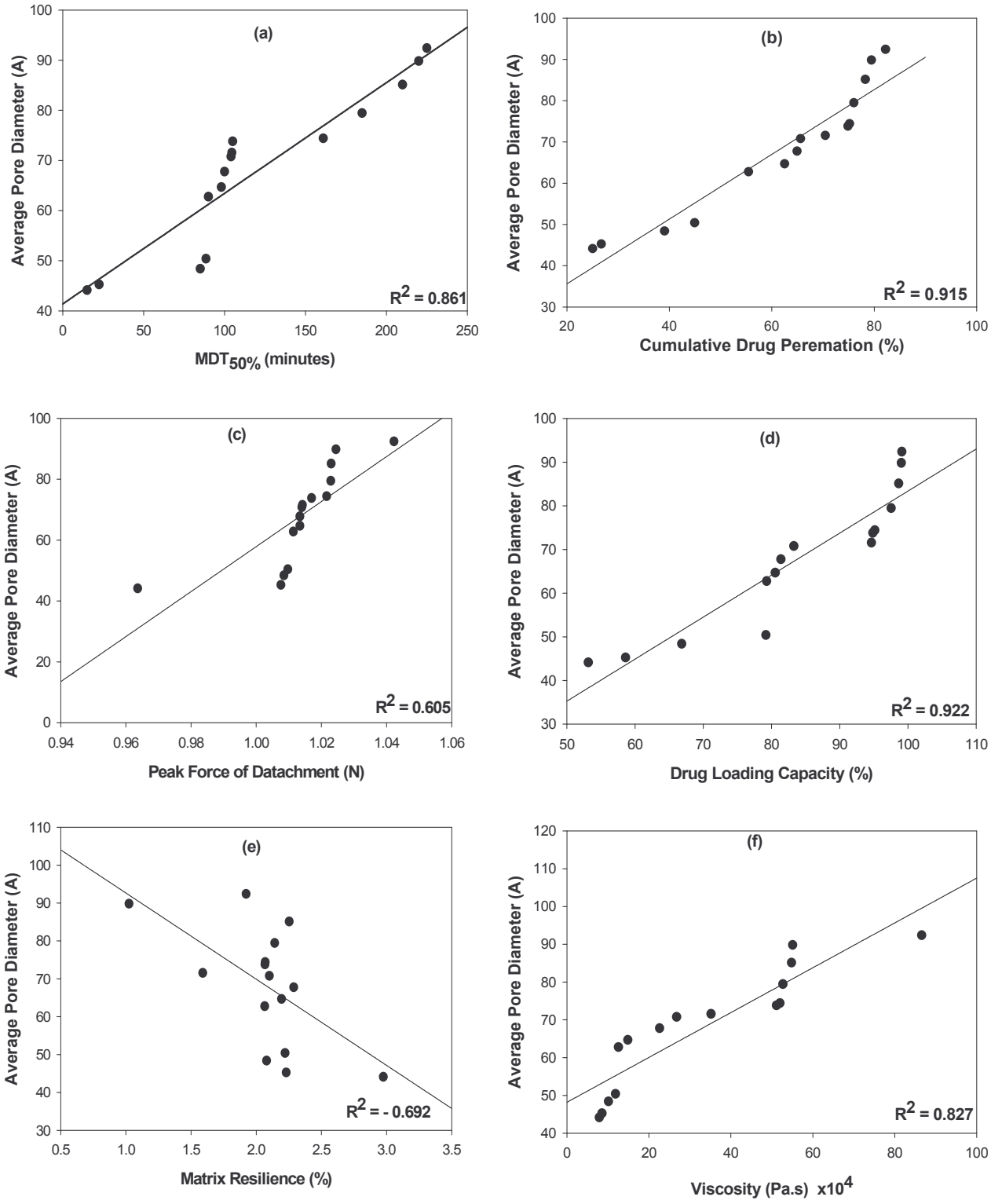

Figure 2.18: Graphical representation showing the direct or inverse linear mathematical relationships between average pore diameter and: (a) mean dissolution time, (b) cumulative drug permeation, (c) peak force of detachment, (d) drug loading capacity, (e) matrix resilience and (f) viscosity.

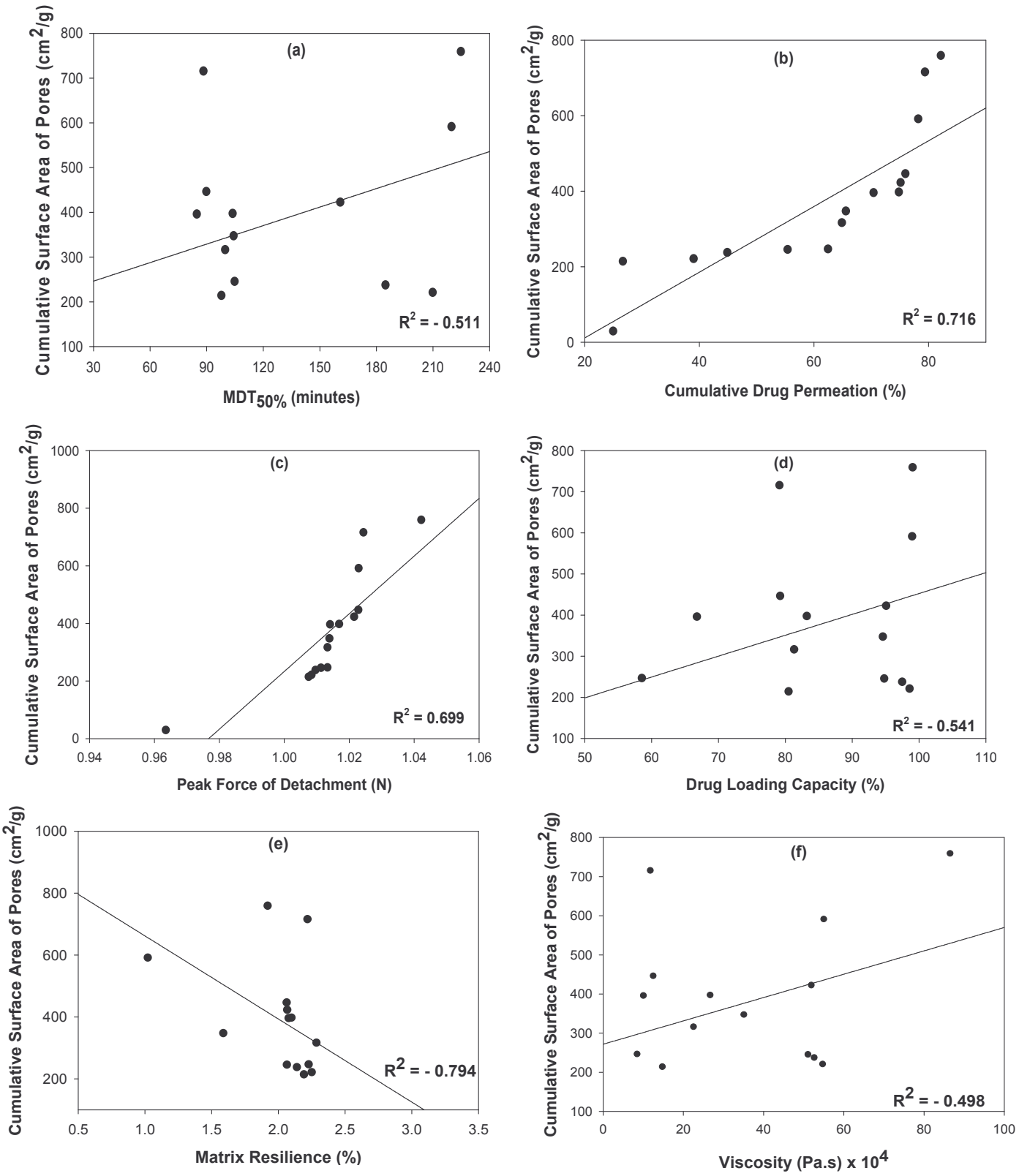

Figure 2.19: Graphical representation showing the direct or inverse linear mathematical relationships between cumulative surface area of pores and: (a) mean dissolution time, (b) cumulative drug permeation, (c) peak force of detachment, (d) drug loading capacity, (e) matrix resilience and (f) viscosity.

2.4. CONCLUDING REMARKS

This experimental phase demonstrated the reliability of the Box-Behnken experimental design as a statistically and mathematically efficient scientific tool for developing the novel pore-regulated polymeric matrices for application in transmucosal drug delivery with respect to the buccal mucosal route of administration. The design employed for the fabrication of the P-RPM revealed the effect of porosity on the magnitude of physicochemical and physicomechanical properties due to the variations in the levels of independent variables employed during the process of fabrication. In addition, ANOVA indicated that the factor levels (independent variables) had significant effects ($p < 0.05$) on the measured response parameters. Interphase, co-particulate, co-solvent, homogenization coupled with pre-freezing and lyophilization proved to be a highly efficient combination of procedures for fabricating the P-RPMs. Also, this methodology had no irreversible distorting influence on the stability, flexibility and viscoelasticity of the homogenous blends employed in the construction of the P-RPMs. This indicates the efficiency of these methods as matrices retained the contributing effects of individual chemical compounds that made-up each formulation. The distinct, changeable physicochemical and physicomechanical characteristics observed with the experimental design formulations imply that the P-RPMs explored in this investigation can be described as flexible systems which make them attractive for the adapted invention and construction of novel drug delivery systems. Statistical analysis of data further confirmed the dependency of the measured physicochemical and physicomechanical response parameters on the independent variables or factor levels ($p \leq 0.05$). As part of this mechanistic evaluation, an optimized P-RPM formulation was constructed based on the information generated. Response parameters selected for the optimization process were those which are related to the intended transbuccal drug delivery application of the formulation and influenced by the distinctive matrix porosity. These response parameters included bioadhesion, drug loading capacity, drug release and cumulative *ex vivo* permeation. The experimental and fitted values generated were closely related, indicating the adequacy and reliability of the statistical design employed. Besides, the direct or indirect impact of quantified porosimetric parameters, namely average pore diameter and cumulative surface area of pores, on the magnitude of selected measured physicochemical and physicomechanical measures such as the mean dissolution time (measure of drug release), bioadhesion, matrix resilience, viscosity, *ex vivo* permeation and drug loading capacity were also observed. Conclusively, an optimized drug-loaded P-RPM formulation was

successfully designed and the investigated physicochemical and physicomechanical properties revealed the potential of this matrix to be applied for sustained transbuccal drug delivery. Furthermore, this chapter employed PS, a class I drug described as having high an aqueous solubility of 100mg/mL at 25°C and permeability of log P = 2.14 as a model drug. In the next chapter, the newly designed optimized P-RPM formulation will be characterized and its versatility with regards to investigating the effects of drug solubility and permeability on the matrix integrity and performance will be explored. Carbamazepine (CBZ), a class II drug exhibiting much lower aqueous solubility (practically insoluble in water) (0.01mg/mL at 25°C) and higher permeability (log P = 2.93) will be introduced as an additional model drug. This will be achieved by quantifying and comparing relevant physicochemical and physicomechanical parameters of the PS and CBZ loaded optimized P-RPMs. In addition the *in vitro* drug release performance of the optimized P-RPM formulation will be compared with that of common commercially available products of PS and CBZ.